Needle Guidance in Clinical Applications based on Electrical Impedance

Håvard Kalvøy

Department of Clinical and Biomedical Engineering
Rikshospitalet, Oslo University Hospital
Norway

Department of Physics
University of Oslo
Norway

Series of dissertations submitted to the
Faculty of Mathematics and Natural Sciences, University of Oslo
No. 960

ISSN 1501-7710

Cover: Inger Sandved Anfinsen.
Printed in Norway: AiT e-dit AS.

Produced in co-operation with Unipub.
The thesis is produced by Unipub merely in connection with the
thesis defence. Kindly direct all inquiries regarding the thesis to the copyright
holder or the unit which grants the doctorate.

Contents

Acknowledgements

The present work was performed at the Department of Clinical and Biomedical Engineering Rikshospitalet, Oslo University Hospital between 2005 and 2010, where I am employed as a senior engineer. The Interventional Centre and the Division of Anesthesiology and Intensive Care Medicine have provided essential contributions, both for clinical support and specialist advices.

I would like to express my gratitude to my supervisors Sverre Grimnes and Ørjan G. Martinsen, whose unique combinations of technical proficiency, scientific judgment, openness to pursue new concepts and gentle personality are highly appreciated.

My sincere thanks to the head of the Department of Clinical and Biomedical Engineering Øystein Jensen, and head of the Section for Research and Development Jan Olav Høgetveit for including me in the great team spirit and for providing good working facilities in the department.

Also, the rest of the staff in the department deserves my gratitude for their professionalism and support, but also for their contributions to the very pleasant working environment.

I am grateful to Audun Stubhaug, at the Division of Anesthesiology and Intensive Care Medicine, for his early enthusiasm and financial support in projects incorporating bioelectric and bioimpedance into clinical practice. This was an important inspiration for conducting the experimental research that initiated the present project. I have been especially pleased with the collaboration with my co-authors Axel R. Sauter and Mike Dodgson from the same division. They deserve special thanks for the inspiration they have given me through their engagement and positive spirit. Through clinical advice and a helping hand, even at short notice, they have been a valuable resource.

The *in vivo* porcine model studies could not been done without the helpful support of Per Kristian Hol and Erik Fosse at the Interventional Centre, who provided excellent facilities for conducting experimental research in an inspiring multidisciplinary environment. Special thanks goes to Lars Frich, who during his employment at the Department of Surgery and the Interventional Centre guided me though my first participations in clinical *in vivo* experiments.

As of my research fellows and co-authors Christian Tronstad, Per Høyum, Bernt Nordbotten and Gorm Krogh Johnsen. It has been a pleasure to cooperate with you, and your academic skills have been a most valuable recourse.

Laerdal Medical AS financially supported parts of this study. I am grateful for their support and especially pleased at being invited into the collaboration with Helge Myklebust, Helge Fossan and Lance B. Becker's resuscitation team at PENN.

My thanks also goes to Dag Sørensen and the staff at the Center for Comparative Medicine who provided excellent care of the animals, and Medinnova AS for their support in administration and patent submission.

My sincere thanks also goes to the volunteers who participated in the clinical study.

Finally, I would like to thank my parents and grand parents who have supported and inspired me over the years. Special thanks to the children Kasper, Silje and Marius, who have been much loved source of joy. I am immensely grateful for the support my beloved Ann has provided during these years. This thesis would not have been possible without her love and patience.

1 Introduction

1.1 Background

A large number of various needle types are in use in clinics today. Typical fields of applications are blood sampling, ablation, biopsy, recording of bioelectrical signals, and administration of drugs. If we extend the definition of needles to include other small or sharp objects for hypodermic placement, e.g. cannulas and small surgical tools, the number of interventions using these types of objects becomes very large.

Quick feedback to secure the correct placement of needles, or other types of these objects, has introduced modern imaging modalities as tools for position guidance. This often introduces relatively large and expressive imaging modalities to the procedures, and specially educated and experienced operators are most often required.

Experimental data published over the years shows characteristic differences in electrical properties between tissue types (Gabriel *et al.* 1996). Our idea was to measure the electrical impedance in a small volume proximal to a needle tip and explore the possibilities to use the characteristic tissue properties to discriminate between tissue types. By determining the tissue type proximal to the tip we could utilize a new method for guidance and to confirm intended needle placements. In principle an impedance measurement requires only moderate electronic circuitry and is often convenient for implementation in relatively small, low cost applications.

If we are able to use small electrodes placed on the tip of the needle, or existing conductive parts on the needles or tools in combination with surface electrodes on the skin, an impedance based guidance method can probably be beneficially implemented in existing devices without any adverse interference on existing procedures. A very simple example can be a green light appearing on the vacuum tube as a nurse hits a vessel during blood sampling.

1.2 Needle guidance today

Every needle used in a clinic has its preferred destination and intended use. It is very infrequently indeed that the position of the needle (or needle tip) is insignificant to the clinician or the patient concerned. In this work we define guidance as support for the user to form an opinion of the situation and to plan further action.

Needle guidance can be done by providing a geometric position on a defined anatomical map or by providing information about the tissue type surrounding the needle tip. This is done to determine if the intended position is obtained, or as part of the complete overview provided to the clinician to understand a situation or for planning further actions.

Discrimination of tissue types surrounding a needle tip cannot give a complete anatomical picture of large tissue volumes, but gives a confirmation if the intended tissue type is localised, as well as the historical path of the needle tip. Stored information of the tissue type the tip has passed through can be compared to anatomical maps to further extend the information provided to the clinician.

Many different techniques have been used over the years. The most used techniques probably involve the nurse that looking for the backflow of blood to confirm the intravenous position of the syringe, or the diabetic patient lifting a skin fold to secure a hit in the subcutaneous fat. However, as the challenges and side effects increase the methods often become more sophisticated. Some commonly used methods are listed below.

Palpation: From training and experience clinicians can determine anatomical positions and place needles in desired positions or tissues from landmarks and palpation. This is an old technique suitable for many clinical procedures, and can be quick and easy for superficial needle placements. Depending only on manual skills, the expense of this method reduces to the salary to the involved personnel. A certain handiness and training is required and success often depends on some feedback to the clinician. Typical feedback can be an abrupt change in the force needed for advancement of the needle, as a different tissue compartment is reached, or backflow of a given body fluid. Our guess is that not too many clinicians would take offence with our assumption that additional guidance (a second opinion from the equipment) would be appreciated, especially in deeper tissues. One of our working hypotheses was that a needle that is able to notify the user when the target position is obtained would be a desired tool.

Stereotaxy: The open content online dictionary, Wiktionary, defines this technique in medicine as: "Stereotaxic surgery: surgery that uses a three-dimensional coordinate system to locate small targets inside the body" (http://en.wiktionary.org/wiki/stereotaxy feb. 2010) Stereotactic techniques for neurosurgical procedures are the most common in use, but in principle the same techniques can be used to direct and move a needle in reference to a three dimensional rigid frame, which can be used to locate a needle tip anywhere in the body. The rigid setup can also give beneficial support in delicate movements during microsurgery.
In general, the major limitation of stereotaxic methods in general is that most parts of the body or tissue not are rigid. Friction in the needle/tissue interface as well as hardly penetrable fascias can cause compression and stretching forces causing the needle push or pull on the tissue. This can cause a local and temporary change in the tissue geometry, which precludes the aiming and insertion accuracy (Abolhassania *et al.* 2006). A needle tip inserted from 3 cm to 4 cm depth and retracted back to 3 cm is not necessarily situated in the same initial tissue. This limits any guidance method (e.g. the ones described below) if it is based on information from a snapshot image taken prior to the insertion. Another disadvantage of the method is the increased invasiveness caused by the mounting the rigid frame on the patient's body.

Ultra Sound (US): Imaging US devices are common in medical clinics today. The technology has evolved towards smaller devices with higher image resolution. An advantage of US is that it can be moved to the patient in almost any examination room and requires minimal preparation. The US involves no ionic radiation and is known for its very few side effects. The two-dimensional visions provided from this modality require needle insertion in the same plane as the image. The operator gets no alert if the needle tip is slightly bent out of this plane. The distal end of the needle reconstructed from echo is not necessarily in coherence with the very tip of the needle. To avoid misjudging the image the operators usually moves the probe and follows objects or boundaries to secure their interpretation of the situation. Because of this the US-modality is often referred to as a dynamic tool, and it is not easily implemented in a robotic system. The method requires a high level of special education and training, and the equipment is relatively expensive.

X-ray/Computer Tomography (CT): Different X-ray modalities are commonly used as a guidance tool today. Typical examples are live angiography commonly used during stenting and other procedures, or arthrography for injection of medication. Recent developments enable three-dimensional images with a very high resolution. Common to all of these is that quite expensive equipment and an especially educated/trained operator (radiologist) is required. Imaging modalities based on ionizing radiation should also be evaluated in the context of patient and operator radiation dose. These methods often imply the use of a contrast

dye. Complications may arise from the use of an injection catheter or from allergic or other reactions on the dye.

Magnetic Resonance Imaging (MRI): The use of MRI has expanded in the last number of years and this modality is superior for tissue type discrimination and reconstruction of high quality images. Expensive and space consuming equipment is required and it is very unlikely that this modality is available in the majority of clinics for a wide range of procedures in near future. Special precautions have to be taken to account for the influence from the magnetic field on the used equipment used, and to avoid attraction of objects into the magnetic field. MRI guiding requires special MRI-compatible equipment that does not interferes with the magnetic field, which distorts the image quality. Regular stainless steel needles can usually not be used. Because of the large coils and the long exposure times, live images during needle insertion are not easily obtained, not even in an interventional MRI. Some patients with implants (e.g. cochlear or pacemakers) cannot undergo MRI and large implants can reduce the amount of information provided by the images.

Electrical nerve stimulation: Today the most commonly used technique to localize peripheral nerves is electrical nerve stimulation. A stimulation needle is connected to a nerve stimulator generating a pulsating electric current. While advancing the needle in the direction of the target nerve, localization of the nerve is confirmed by the observation of muscle twitches, induced by a depolarization of the nerves by the electrical current. After localizing the nerve, the injection of anaesthetics is done through the hollow stimulation needle. This is an efficient method that only requires only a small hand held low cost stimulator. The relation between stimulation current and distance to nerve is discussed, and we hope some of our results can contribute to enhanced knowledge about the method.

1.3 Electrical bioimpedance

Bioimpedance is a passive electrical property that deals with biological material's ability to oppose (*impede*) electrical current. *Bioelectricity* deals with active electrical properties and the tissues ability to generate or respond to electricity. Examples can be the electrical activity of the heart (electrocardiography) or an action potential from a nerve. This can be measured *endogenically* which means picking up signals generated by the tissue.

Passive electrical properties, such as *Bioimpedance,* can only be measured *exogenically*: as a response to a known electric excitation. The excitation can either be a current or a potential galvanic coupled to a volume of the tissue by electrodes. A galvanic coupling through the same or other electrodes then picks up the response. By applying a current and detecting the potential over a tissue volume, we get the resulting *impedance* of that volume. The inverse of *impedance* is called *admittance* and is obtained by applying a potential and detecting the current through the tissue volume (all mathematical definitions and the relation between them are given in the appendix). It is not always obvious if impedance or admittance is best suited, so the term *immittance* is sometimes used to unify both models.

The transfer of charge (current) in the metal leads and electrical components of the measurement equipment is caused by the movement of electrons, but in the tissue the main charge carriers are ions. The transfer from electronic to ionic charge carrying occurs at the electrode interface. This transfer gives rise to an electrical double layer, half cell potential and can result in a high impedance at the electrode/tissue interface, which can be reflected in the measurements. Due to these properties of the electrodes, great care must be taken in their placement to obtain genuine and undistorted tissue data.

The membranes of living cells consist mainly of a thin lipid layer (~7 nm) penetrated by different ion channels for controlled transport of ions and substances necessary for the metabolism of the cell. The membrane is often described as semi-permeable since certain ions are allowed to pass and others are not. This gives the membrane a high capacitance (~1 $\mu F/cm^2$) and a low but complicated pattern of conductivity (~10^{-6} S/m) (Grimnes and Martinsen 2008). The extra- and intracellular environments consist mainly of aqueous electrolytes with important resistive properties. The capacitive properties allows high frequency current to pass the membrane into the intracellular fluid, but as the frequency decreases more of the current will pass around the cells in the extracellular fluid (fig. 1). If no active response occurs in the tissue, this implies that the impedance of the tissue will increase as the frequency decreases.

Inductive properties can also be found in biological tissue, but as commented by Riu (2004) the inductance at frequencies below 10 MHz is usually insignificantly low compared to the resistance and reactance commonly found in the human body.

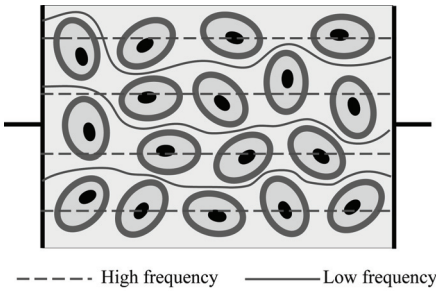

Figure 1: The current flows through the cells if the frequency is sufficiently high. More of the current must pass between the cells as the current decreases. This is the main mechanism behind the β-dispersion (fig. 2) and is an example of frequency dependent properties of tissue.

Tissue is a very heterogeneous material, and interfacial processes are very important. Different types of tissue, body fluids and the parenchyma of organs, can have very different cell structures. Both the size and shape of the cells, and the binding between the cells shows large variation. Adipose tissue has tight bound cells with little extracellular electrolyte for conduction of LF currents. Other tissues and body fluids can have less cellular density or can be pure electrolytes. Fascias and skeletal muscles can give the tissue anisotropic properties. Bound polarisable molecules and the movement of charge along membranes can give the tissue dielectric properties with characteristic time constants. Many such differences can have significant influence on the measured impedance and how it changes with the measurement frequencies.

Schwan (1957) explained some of the mechanisms behind the dielectric dispersions in the context of bioimpedance and divided the relaxation mechanisms into three groups; α-, β- and γ-dispersions (fig. 2). More on this and the electric properties of cells and tissue can be found in Grimnes and Martinsen 2008. In bode plots (see fig. 2 and sec. 1.4) a distinct fall in modulus between two plateaus and a corresponding rise in the phase shift can be seen around the characteristic frequency of the dispersion. In Wessel-plots (see fig. 3 and sec. 1.4) dispersions can be seen as circular elements.

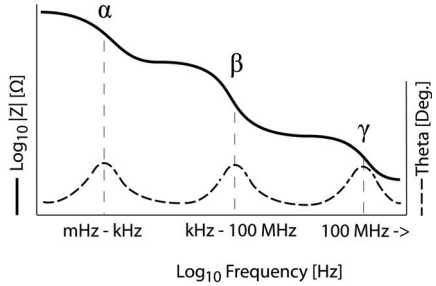

Figure 2: Typical modulus and phase angle as function of frequency for α-, β- and γ-dispersion.

Impedance measurements as modality to provide images of the human body have been a hot topic during the last decades. The method is called Electrical Impedance Tomography (EIT) and the images are obtained from reconstruction algorithms and transfer impedance measurements from a number of surface electrodes placed on the skin of a patient. Together with the number of electrodes and quality of the algorithm, the resolution of the image is dependent on the distance from the electrodes. The method is further explained and firmly reviewed by Brown (2003). In general impedance measurement methods are known to utilise inexpensive equipment with low hazard rate, and can in most cases be implemented in small device.

1.4 Numerical analysis of impedance data

Wessel plot
Complex numbers plotted with the real part (Re) on the X-axis and the imaginary part (Im or j) on the Y-axis, are frequently used to plot the positions of the poles and zeroes of a function in the complex plane. In the field of bioimpedance these plots are used for analysis and curve fitting of measured or simulated impedance (fig. 3). Similar plots are also used for admittance models by plotting conductance on the real axis and susceptance on the imaginary axis. Jean-Robert Argand (1768-1822) is probably the best known among the early users of complex plane plots, but such plots were also used by a former engineer at Bell Laboratories, Harry Nyquist (1889–1976), and the Norwegian land surveyor and mathematician Caspar Wessel (1745-1818). We here use the term Wessel plot here, after the first known user.

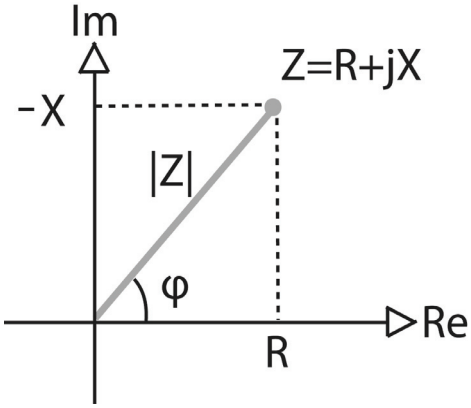

Figure 3: Wessel-plot of a general impedance (Z). The minus on the X indicate that the imaginary axis (Im) is inversed to keep the vector inside the first quadrant of the plot for typical capacitive bio-samples. (The symbols are defined in the appendix.)

Bode plot
In fig. 2 we have plotted the modulus and phase angle as function of frequency (impedance spectre). Logarithmic scale on the abscissa (X-axis) is commonly used to enhance the readability over a wide range of frequencies. For systems where the measured modulus spans more than a decade of ohms, it is also common to use logarithmic Y-axis. The logarithmic scale is also convenient for curve fitting to Fricke's law (Fricke 1932) or a constant phase element (CPE, eq. 1 or eq. 2) used in the Cole-model (eq. 3). Both have exponential relations to frequency, which can be estimated by fitting a straight line in a logarithmic plot (Schwan 1992, Khambete *et al*. 1995, Raicu *et al.* 1998 and Bordi *et al*. 2001). The phase angle is typically 0 to 90 degrees for an admittance model and 0 to -90 degrees for an impedance model. Because of this the phase plotted on the ordinate (Y-axis) usually is linear, and due to the negative phase angle an inverse Y-scale is quite common for impedance models.

Cole model
Kenneth S. Cole developed his empirical equivalent model (fig. 4) from curve fitting to a large amount of measurements (Cole 1940). The model is widely used as a general model for a one dispersion system. More complex systems, with more than one dispersion, can be modelled by using additional Cole-elements.

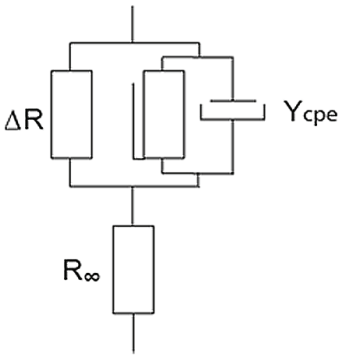

Figure 4: Commonly used equivalent circuit compatible with the Cole model.

Frequency spectra from biological matter often have a characteristic frequency independent phase angle in parts of the spectrum. Since this behaviour is not possible to model with a finite number of ideal resistances and capacitances, the Constant Phase Element (CPE) is included in the model. Mathematically this component is defined by setting φ_{CPE} to a constant value, which implies that the real and imaginary part of the CPE must be dependent on the frequency in the same way. Grimnes and Martinsen (2008) showed that the CPE can be described as an impedance (Z_{CPE}) or an admittance (Y_{CPE}) as below.

$$Z_{CPE} = R'(j\omega\tau)^{-\alpha} \qquad \textbf{Eq. 1}$$

$$Y_{CPE} = G'(j\omega\tau)^{\alpha} \qquad \textbf{Eq. 2}$$

R' and G' is a resistance and a conductance given in Ω and S, respectively, ω is the angular frequency (2πf), τ is the characteristic time constant and α is an exponent with relations to the phase angle.
The equivalent circuit in fig. 4 is described by the Cole equation as:

$$Z = R_{\infty} + \frac{\Delta R}{1 + (j\omega\tau)^{\alpha}} \qquad \textbf{Eq. 3}$$

$$\Delta R = R_0 + R_{\infty}$$

where the impedance (Z) of the system is given by Y_{CPE} (eq. 2) and the resistance at zero (R_0) and infinite (R_∞) frequency. This equation implies that G' in eq. 2 must be defined as $1/\Delta R$. This is not always the case, and by allowing G' to be independent of ΔR Grimnes & Martinsen (2005) have modified the equation for better fit to general relaxation theory. Working on permittive systems Cole also developed the Cole-Cole equation together with his brother, Robert H. Cole (Cole and Cole 1941). This equation describes permittive systems in a similar manner as the Cole-equation describes impeditive systems.

Kramers-Kronig Transforms

Based on mathematical analysis Kramers-Kronig proved their transformation between the real and imaginary part in a linear network function (Riu and Lapaz 1999). This theoretical relationship states that in a passive, linear, reciprocal network (Grinmes and Martinsen 2008) there is no additional information in, for example, the real part if the imaginary part is known

for all frequencies. Riu and Lapaz (1999) have showed how this theory can be applied to measured bioimpedance data, and how it can be used in validity testing of measurement setups and data. Noise, poor electrode contact or other parasitic elements and nonlinear behaviour, can easily be identified and eliminated by checking a set of measured resistance and reactance spectra (or conductance and susceptance in an admittance model) in accordance with this theory.

Sensitivity estimation

The measurement sensitivity in a given point in the sample (voxel) is found from the following equation:

$$S = J'_{reci} \cdot J'_{cc} \quad [1/m^4]$$

Eq. 4

Here the J'_{cc} is the unity current density vector (local current density vector divided by the total excitation current) in the voxel set up by the excitation signal from the current carrying electrodes. J'_{reci} is the theoretical reciprocal unity current density vector. This vector is given from the current density expected in the voxel if we switched the electrode pairs and used the pickup electrodes to transfer the excitation signal. The spatial sensitivity for a given measurement setup can be calculated for a single voxel from eq. 5. Examples of calculated spatial sensitivity distribution are found in fig. 6 and 7. The contribution from one voxel in the total impedance of the setup is given by impedance volume density (ρS dv) given by the local sensitivity, resistivity (ρ) and dv the (infinitesimal) volume of the voxel. In a monopolar or bipolar setup the reciprocal current is identical to the excitation current and J'_{reci} equals J'_{cc}. Thus, the sensitivity for a given point is given by the squared local unity current density ($S=|J'|^2$). The total impedance (Z) of a setup can be found by integrating over all voxels according to:

$$Z = \iiint \rho |J'|^2 \, dv \qquad [\Omega]$$

Eq. 5

In some simplified cases if the geometry of a setup is close to ideal models the spatial sensitivity can be estimated by analytical calculations. A relevant example is a spherical electrode in a homogenous medium where the sensitivity is inversely proportional to the radius of the volume centred in the sphere. This and other examples of analytical estimation are found in Grimnes and Martinsen (2008). Exact determination of local resistivity and geometry is not always possible in real samples, but good estimates of the sensitivity field can often be found from calculations based on approximations to analytical solutions or eq. 6.

Multivariate analysis (techniques)

Multivariate analysis is a collection of statistical and mathematical methods used in statistical analysis of more than one variable at a time, in datasets involving multiple observations. Most of the methods are well established calculations implemented in various mathematical software packages and explained in basic statistical literature (e.g. Wikipedia.org presents articles and further references on the topic). In the presented work we used the 'Unscrambler® 9.7' software, and two of the most relevant methods are summarized below.

Principal Component Analysis (PCA)

PCA is a mathematical procedure (orthogonal linear transformation) used in multivariate analysis to transform a number of possibly correlated variables into a smaller number of uncorrelated variables called Principal Components (PC). The first PC accounts for as much of the variability in the data as possible, and each succeeding component accounts for as much

of the remaining variability as possible. The main aim is to reduce dimensionality of a data set with a minimum loss of information. If a multivariate dataset is visualised as a set of coordinates in a high-dimensional data space, PCA supplies the PC as a lower-dimensional picture, a "shadow" of the dataset viewed from its most informative viewpoint. In a discriminate analysis (e.g. tissue discrimination) it will often be beneficial to simplify a high-dimensional data space into the least number of PC that can facilitate the desired discrimination in a reliable way.

Partial Least Square Discriminate analysis (PLS)
PLS is a statistical method with some relation to principal components analysis; instead of finding PC's with maximum variance between the response and independent variables, it finds a linear regression model by projecting the predicted variables (X) and the observable variables (Y) to a new PC-space. The X variables (the predictors) are reduced to PC's, as are the Y variables (the dependents). The components of X are used to predict the scores on the (measured?) Y components. This can be visualized in a score plot.
In a predictive model the Y component scores are used to predict the actual values of the Y variables. In constructing the PCs of X, the PLS algorithm iteratively maximizes the strength of the relation of successive pairs of X and Y component scores by maximizing the covariance of each X-score with the Y variables.
PLS-regression is particularly suited when the matrix of predictors has more variables than observations.

1.5 Needle electrodes

Needle electrodes are common tools in many clinical procedures today. A wide range of types and sizes are commercially available from a large number of manufacturers and distributors. The applications are usually restricted to pick up some kind of bioelectrical potential or stimulation of tissue. Appropriate mechanical characteristics are essential for clinical needle electrodes both for facilitating the intended insertion path (Abolhassania *et al.* 2006) and to apply to safety regulations. Throughout the present work the focus has been on the electrical properties. Needles for different applications with prospects for invasive impedance measurements are listed below.

Insulated massif needles

A typical use of insulated massif needle electrodes is Electro Myo-Graphy (EMG) where action potentials from afferent nerve fibres are picked up for monitoring of muscle activity (King *et al.* 1996). To obtain potential readings of high spatial sensitivity in the active electrode there is a small part of the tip that is not insulated. Typical 24 to 28G and length from 25 to 75 mm, with active areas are from a few mm^2 and less.

Hollow needles for Peripheral Nerve Block (PNB)

PNB procedures are probably one of the most common applications for hollow needle electrodes. Most of the used needle types are insulated hollow needles with some kind of exposed non-insulated tip used as the active electrode area. These needle electrodes are used to stimulate tissue for locating selected nerves before the same needle is used for administration of drugs. Typically from 18G to 22G thick, 50 mm to 150 mm long stainless steel electrodes, with active electrode areas from very small pinpoint and up to about 1 mm (Dalrymple and Chelliah 2006). Similar needles are also used as injectable EMG electrodes (typical 22G to 30G and 25 mm to100 mm length).

Ablation needles

The most common needle used in surgical ablation is a hollow electrical needle, which is electrical insulated except for the distal end. But a variety of needles and electrodes are used for monopolar and bipolar ablation. Jonson *et al.* 2005 show some examples. Stimulation and impedance measurement is done in the surrounding tissue. Impedance is usually measured at the same radio frequency as the stimulation signal, and used to evaluate the placement of the electrode and the progression of the ablation.

Concentric

A different number of electrodes can be mounted at the tip of a needle. These needles are often made with a flat or bevel area on the tip with a central point electrode and one or more concentric rings in different radius form the middle with insulation between (Khambete *et al.* 1995 and King *et al.* 1996). These types of electrodes are made in a wide range of sizes from large macro electrodes for surface measurements to small microelectrodes mounted on needles. Typical examples are concentric bipolar needle electrodes for EMG. These come in different materials, but are typically made of stainless steel with platinum core electrode, with sizes from 23G to 30G and 25mm to 75mm length.

Ring electrodes

Needles with one or more ring (bands) electrodes mounted along the shaft have been used for measurement in different setups (e.g. fig. 7.43 in Grimnes and Martinsen 2008). The most common setup is rings with the same radius and width equally separated along the needle.

Multiple microelectrode needles

Two or more needles can be mounted in an array for subcutaneous measurements. These can be insulated or not and the measurement can be done between the needles or in reference to other electrodes e.g. on the surface. Such methods can be used to make needles containing large number of microelectrodes for a variety of applications e.g. Ulbert *et al*. 2001. Some examples are also illustrated in Grimnes and Martinsen 2008 (sec. 7.4.7).

Venflon/microdialysis-catheter

Venflons, catheters and cannulas made of non-conducting materials can be use for impedance measurements if they are filled with an electrically conductive coupling fluid connected to an electrode This principle is similar to the coupling fluid method explained in sec. 1.7 and by Schwan (1966).

1.6 Electrode configurations

Appropriate configuration and design of electrodes can be a crucial factor for success in the development of a new application. The most common configurations are 2-, 3- and 4-electrode setups. In this section we have illustrated some of the properties of these setups in two dimensional finite elements simulations (FEM) done in Comsol Multiphysics (Comsol AB). Two-dimensional setups are not possible in the real world, but the simulations can be interpreted as a cross section of setups with very large (infinite) depth. In these setups the electrodes will be long rods oriented with the long axis perpendicular to the plotted cross section.

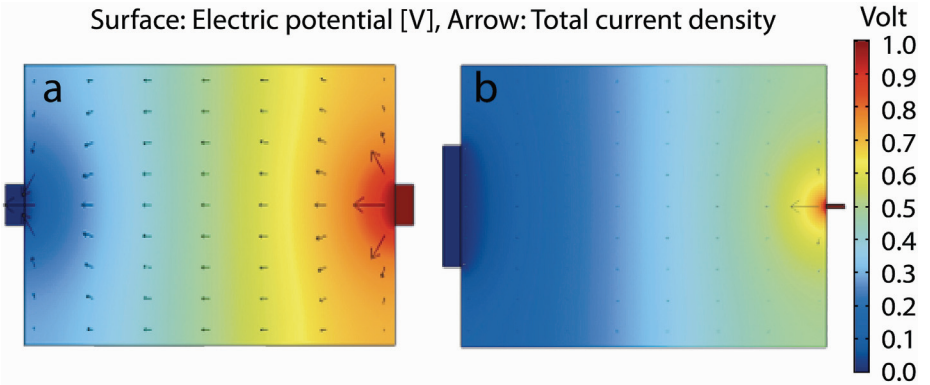

Figure 5: Current density and potential distribution in 2-electrode systems. The same pair of electrodes is used for excitation and pickup. The measured impedance is the sum of impedance in the leads, electrode interfaces and the sample. **a**: Symmetric setup, **b:** Quasi-Monopolar setup obtained by large difference in active electrode area.

2-electrode setup

A 2-electrode setup gives a one-port measurements system. The same pair of electrodes are used both for excitation and measurement. The impedance of the complete system of electrodes and sample are found by applying a controlled potential excitation signal between the electrodes and measuring the current through the leads. The measurement is done along the current path through the whole setup, and the sample, the electrode interfaces, the electrodes and the connection leads will contribute to the impedance in series. In a similar manner applying a current signal and measuring the potential difference between the electrodes gives the admittance of the setup.

Fig. 5a illustrates a symmetric 2-electrode setup (bipolar) with ideal electrodes of same size. The potential distribution is given from the colour bar and current density is illustrated by the size of the arrows. Highest current density and largest potential drop are found proximal to the electrodes, giving an enhanced sensitivity (ref. eq. 5) in the constrictive zone (further described by Grimnes and Martinsen 2008). In the corners of the sample the arrows almost vanish, indicating an insignificant contribution from these volumes. In the rest of the volume (bulk saline) the current density is quite evenly distributed resulting in an almost homogenous impedance volume density. The relative difference in sensitivity between the corners and the constructional zone will decrease if the electrode size is increased towards the sample size. By doing the opposite, decrease the size of one of the electrodes, the relative difference is increased. If the other electrode is sufficiently large the impedance contribution from this electrode can be made insignificantly small. With these modifications we can obtain a quasi-monopolar setup, with one small active measuring electrode and one large indifferent electrode as illustrated by the simulation result plotted in fig. 5b.

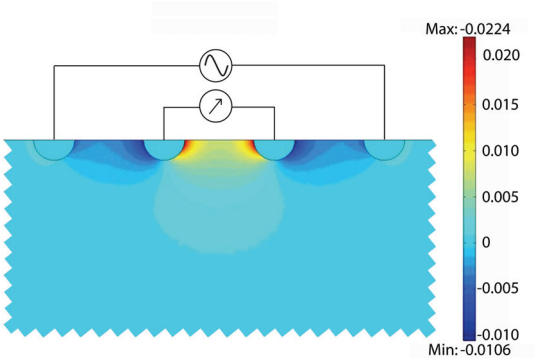

Figure 6: Sensitivity plot for a 4-electrode setup in an infinite homogenous medium. Be aware of the negative sensitivity zones (blue) and the light blue zero sensitivity in the bulk.

4-electrode setup

By using two pairs of electrodes, one pair for current carrying and one for pick-up (two-port network), current through the measuring electrode and parasitic properties in these can be avoided. The current through the tissue between the current carrying electrodes sets up a potential over the tissue proportional to the impedance in the tissue. If the input impedance in the signal amplifier connected to the pick-up electrodes is sufficiently high and no current flows in their leads, the potential difference between these can be picked up without influence from EPI. If a controlled current signal within the linear region is used for excitation the impedance is proportional to this potential. A typical 4-electrode setup is illustrated in the sensitivity distribution plot in fig. 6. The spatial sensitivity in a large (infinite) homogenous sample is simulated from eq. 5, and illustrated by the colours as found in the colour bar. Schwan and Ferris (1968) explain 4-electrode measurements in more detail, and Grimnes and Martinsen (2007) discuss the negative sensitivity found in fig. 6 and some of the pitfalls of this type of setup.

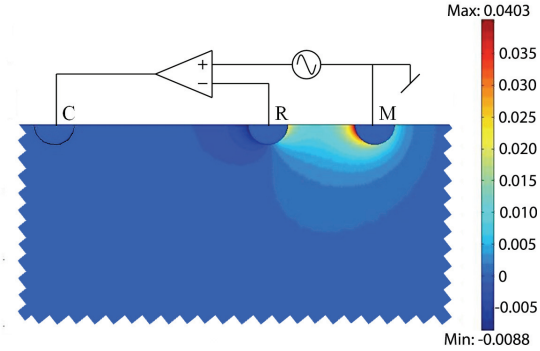

Figure 7: Sensitivity plot for a 3-electrode setup in an infinite homogenous medium. Zero sensitivity (blue) everywhere except between the reference (R) and the measuring electrode (M) and in the vicinity of M. Current carrying electrode (C) is truly indifferent. Similar to the 2-electrode system in fig. 5b the 3-electrode can utilizes monopolar measurement by reducing the relative size of M.

3-electrode systems

A 3-electrode system is setup by using one pair of electrodes for current carrying and one additional electrode to measure the potential between one of the current carrying electrodes (the measuring electrode, M) and the reference electrode. Since no current can flow through the reference electrode, its input impedance can be made very large to avoid influence form this electrode in the measurement (Grimnes 1983). The measurements done with this setup will reflect the impedance in the sample between the reference electrode and the measurement electrode. The measurement electrode interface and the properties of this will be included in the measurement.

By decreasing the size of the measuring electrode the measurement will be monopolar in the same way as in fig. 5b, but the size of the indifferent electrodes will be less crucial.

1.7 Electrode polarization impedance and methods to correct for electrode effects

Electrode polarization impedance (EPI) is a common problem in low frequency electrical bioimpedance measurements (Schwan 1966 and 1992, Gabriel *et al.*1996, Mirtaheri *et al.* 2005, Bordi *et al.* 2001, Raicu *et al.* 1998 Davey *et al.* 1990, McAdams *et al.* 1995, Stoneman *et al.* 2007 and Geddes *et al.* 1971). The EPI becomes more pronounced in highly conductive media (Schwan 1992, Gabriel *et al.* 1996, Bordi *et al.* 2001) or when using small electrodes (Schwan 1992). By using needle electrodes we expected significant influence from EPI, and methods to reduce unwanted electrode properties were evaluated. The result of our literature survey on this topic is given in this section.

Schwan (1992) résumés the history of the EPI since it was first described over a century ago. Along with others he refers to different models for describing the behaviour of the EPI. The most common models are:

i) A frequency dependent resistor and capacitor ($R_p(\omega)$ and $C_p(\omega)$) in series (Schwan 1992, Raicu *et al.* 1998)
ii) A frequency dependent resistor and capacitor in parallel (Davey *et al.* 1990)
iii) A Cole circuit or similar (Schwan 1992)
iv) A Constant Phase Element (CPE) (Bordi *et al.* 2001, McAdams *et al.* 1995 and Stoneman *et al.* 2007)
v) A permittivity model similar to the Cole-Cole equation (Schwan 1992 and Davey *et al.* 1990).

All of these connected in series with the sample under investigation.

Below we list a short summary of different techniques for minimization or correction of the EPI influence on impedance measurement proposed over the years.

A Mathematical subtraction:

Many investigators have estimated the contribution from EPI and sample data in their measurement data by fitting to theoretical models (e.g. points i) to v) described above). This way the constituent under investigation can be extracted. (Mirtaheri *et al.* 2005, Geddes *et al.*1971) The most common is to fit the EPI to frequency dependent R_p and C_p connected in series (model i)) (Schwan 1992, Raicu *et al.* 1998) or to a CPE (Stoneman *et al.* 2007 Bordi *et al*. 2001 and Raicu *et al.* 1998), but all the models described above and probably also others have been used. This can be done with linear regression and extrapolation in a double logarithmic plot of the measured resistance and capacitance, a bode plot of modulus and phase, or by fitting a Cole element in a Wessel-plot (Grimnes and Martinsen 2008).

B Electrode distance variation

In a homogenous cylindrical sample with circular disc electrodes covering the ends, the measured impedance will increase with the length of the cylinder. If the distance between the electrodes is sufficiently large, the EPI will be constant. A difference in impedance caused by a variation of the electrode distance can only be due to the change in the sample impedance. From the linear relation to length the sample impedance can be calculated and separated from the EPI (Schwan 1992, Geddes *et al.* 1971).

C Substitution method

A sample under investigation can be substituted by a calibration solution with known impedance properties. If the calibration solution is chosen to approximate the EPI in the sample measurement, the properties of the investigated sample can be found by subtracting the EPI determined in the calibration measurement (Gabriel *et al.* 1996 and Davey *et al.* 1990). Since the EPI has been shown to be sample dependent (Schwan 1992, Gabriel *et al.* 1996, Mirtaheri *et al.* 2005 and Bordi *et al.* 2005), this method should only be used if the concentration of particles in the sample is low (Grimnes and Martinsen 2008)(e.g. volum fraction <0.10 (Stoneman *et al.* 2007)).

D 4-electrode

By introducing one pair of electrodes for picking up potential in addition to one pair of electrodes for current carrying, the 4-electrode technique can eliminate most of the problem with EPI. This is a widely used method described by Schwan and Ferris (1968), but there are some pitfalls that are not well-known, as described by Grimnes and Martinsen (2007).

E Increased current densities

The electrode impedance is dependent on current density. Above a certain limit of linearity the impedance falls with increasing current densities (Schwan 1992, s 217, Geddes *et al.* 1971). This can be used to reduce the EPI, but is rarely used since the potential/current relationship is nonlinear at this current density level.

F Electrode modification

By changing the electrode geometry, material or surface structure, the properties of the electrode/tissue interface can be modified and the EPI can be reduced substantially (Schwan 1992, Mirtaheri *et al.* 2005, Stoneman *et al.* 2007, Grimnes and Martinsen 2008). A typical example is increasing the roughness of the electrode surface and the use of platinum black (Grimnes and Martinsen 2008).

G Reduction of sample conductivity

Because EPI is most pronounced in measurements in highly conductive media (Schwan 1992, Davey *et al.* 1998), a reduction of sample conductivity will reduce its influence. (e.g. by increasing the number of cells in a suspension).

H Electrodeless excitation by magnetic induction instead of contact electrodes

The electrodes and their errors can be avoided by using a coil and magnetic induction for excitation of Eddy currents in the sample. Earlier investigations (McAdams *et al.* 1995, Geddes *et al.* 1971 and Scharfetter *et al.* 2003) have described this method and concluded that since the sensitivity is decreasing with frequency, this method is not feasible for frequencies below 10 kHz.

I Coupling fluid

Schwan (1966) has demonstrated how the electric contact between an electrode and a measurement point can be established by using a coupling fluid, and how this can be used to reduce the effect of electrode polarization. The influence from a pickup electrode can be avoided by moving the electrode out of the current field, and the current carrying electrodes can be enlarged to reduce the EPI (as discussed above). If the contact area between the coupling fluid and the measured sample is kept small the focus of the current or the potential measurement point can be preserved.

Intuitively the best approach is to modify the measurement setup to reduce or eliminate the effect from EPI before measuring. Methods D, F, H and I are of such character, and one rule of thumb could be to always consider these methods and evaluate measurement setups in pilot studies before resources are used for further collection of data. Method I requires a hollow needle and a high series resistance will be introduced if used on a thin needle. Because method H requires larger and more complex measurement setups, it is not well suited for our applications. Method D and F have long traditions of use in a variety of impedance measurements and could probably also be used to reduce the EPI in our application. But by aiming for maximal impact in clinical application, our focus has been to prove the feasibility of the method using commercially available needles already in clinical use. This leaves us with method A if the EPI is to be reduced.

2 Aims of the study

The aims of this study were to develop and determine the feasibility of a new method for needle guidance in clinical applications based on electrical impedance used for tissue discrimination.

The aims of each paper are found in the reprints of the Paper I-VI.

Sub-goals were:

- ✓ Gathering tissue type specific impedance *in vivo*
- ✓ Determine if characteristic differences between tissue types are sufficient for discrimination
- ✓ Gathering fundamental electric properties of needle electrodes
- ✓ Implementing fundamental knowledge of electrodes and electrode setups in simulation models for use in application development
- ✓ Determine if adequate spatial sensitivity is obtainable
- ✓ Find suitable electrodes and electrode setups
- ✓ Demonstrate the feasibility of the method by showing an application example

3 Materials and methods

In this section we describe the core equipment used in more than one of the experimental studies, and some of the pilot studies done during the planning of the project and the design of the studies. Descriptions of different kinds of equipment used solely in one of the studies are found in the reprints of the published papers.

3.1 Core equipment

All impedance measurements in the studies I-VI were obtained using a Solartron impedance measurement system; a Solartron 1260 Impedance/Gain-phase Analyzer and a Solatron 1260 impedance interface (fig. 8). A regular Laptop was connected to the Solartron 1260 to control the system and for storing data.

Figure 8: Solartron 1260 (left) and 1294 (right)

The system has two sets of output/input ports, one set of ordinary (non-medical) connections and one set approved for medical use (IEC601). We used the non-medical connections for all *in vitro* and all *in vivo* porcine model measurements. The medical connections were used on human volunteers in study II.

Solartron 1260	Solartron 1294
Frequency range 10microHz to 32MHz. Frequency resolution: 1 in 65million (0.015ppm). 0.1%, 0.1° accuracy. Resolution to 0.001dB, 0.01°. Measures impedances >100Mohms. 2-, 3- and 4-terminal measurement configurations. Polarization voltage up to ±40.95V.	Sensitivity 1µV, 1pA. Impedance range 10^{-2} to >1GΩ.

Table 1: Manufacturers specifications

Lock-in-amplifier
The Solartron 1260/1294 measurement system includes a Lock-in-amplifier, which is commonly used to detect small signals buried in noise. A very efficient reduction of noise is obtained by excluding all signals not perfectly synchronized with a defined reference signal. The noise reduced measurement result is obtained by averaging the signal in phase with the reference over a period of time. Dependent on the measured setup, the resistance or conductance of an impedance or admittance is found by using a reference in phase with the excitation signal. The 90 degrees out of phase component (reactance and susceptance) is found the same way by introducing a phase shifted reference signal. Frequency spectra are obtained from repeated measurements where the frequency is adjusted in given steps between each averaging period. The noise reduction rate is dependent of the number of averaged cycles, and the difference between the measurement frequency and the frequency of the noise (Grimnes and Martinsen 2008).

Software
The software for setting up the Solartron system for measurement and analyzing resulting measurement data is provided by Scribner Associates inc., North Carolina.

The Zplot-software is used to control and setup the Solartron system for different measurement protocols and to save the measurement data in the file system. It provides controlled current or controlled potential excitation signals of different amplitude. Measurement series can be setup as sweep of time, frequencies, amplitude or DC offset, or as batch files. Different measurement accuracy can be obtained by manipulation of type of integration or integration time. A limitation of the system is that, even if the frequency can be swept, it is not possible to measure at more than one frequency at the time.

The software Zview is used to display and analyze the measurement results. Data can be plotted in a wide range of Wessel- and Bode-plots with axis displaying different values extracted from different impedance and admittance models. Different methods for curve fitting are available in the different types of plots. Equivalent circuits can be built for fitting to freely designed models, or simple equivalent models can be found in libraries for instant fitting.

Ultra sound comparison
We used US as the gold standard comparison for all the *in vivo* measurements. In Study I, Study VI and all *in vivo* pilot measurements we used Vingmed system FiVe (General Electric–Vingmed, Milwaukee, Wisconsin). On the volunteers in Study II we used Philips iU22 ultrasound unit (Philips Medical Systems, Bothell, WA).

Electrodes
For large impact in the clinic we aimed at for using equipment already in use in clinics today. At project start up we did not know if this was feasible, or if special electrodes would have to be made. Specially designed needles with multiple electrodes near the tip make it possible to choose between 3-, 4- or bipolar 2-electrode setups (fig. 5, 6 and 7), and to manipulate with the size and distance between the electrodes to control the sensitivity. After testing a wide range of electrodes of the types described in sec. 1.5, we found that needles electrodes with insulated shafts gave the best results and ended with the electrodes described below for further investigations. If the feasibility of the method could be proven with these needles then no specially designed electrodes would be necessary at this stage.

Needle electrodes

Almost all needles for clinical use are made of stainless steel. Mirtaheri *et al.* 2005 reported significant differences in electrode properties between metal types. The electrode properties of stainless steel was not found to be more suited than any other material, but probably because of its mechanical strength the majority of clinical needles are made of stainless steel. The active electrode area is also most often an exposed part of stainless steel, but plating of gold or other metals is sometimes used to obtain other active electrode properties. In the present work we picked six types of commercially available medical grade stainless steel needle electrodes (medical grade is defined in Paper III). Four of which were massive monopolar EMG electrodes (four rightmost in fig. 9) and two were hollow needle electrodes for PNB (illustrated in fig. 13 and leftmost needle in fig. 9).

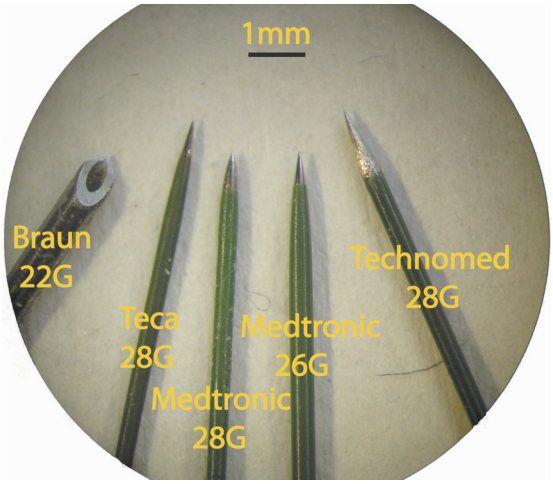

Figure 9: Zoomed image of the studied needles. Together with the Stimuplex D needles sketch in fig. 13 these are all used needles.

Reference electrodes

The *in vitro* experiments involving stimulation of the electrodes were done with different stainless steel plates and cylinders as explained in detail for each setup. 'Blue sensor' Q-00-A, (Ambu Medicotest A/S, DK) were used as current carrying and reference electrodes in all *in vivo* measurements and other measurements where 3-electrode setups were used. These were Ag/AgCl electrodes with active electrode area approx. 60 mm^2 (Ø=19mm). In the *in vivo* measurements these were placed on the skin near the measured tissue volume. To ensure full contact, the skin was shaved before placement, and the placement was picked so that no unnecessary tissue series impedance was introduced.

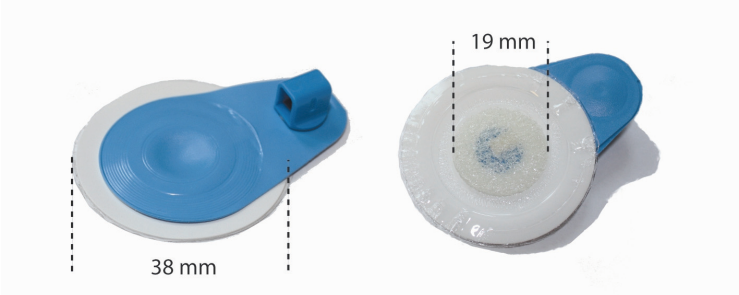

Figure 10: 'Blue sensor' Q-00-A Ag/AgCl surface electrodes used as current carrying and reference electrodes.

3.2 Pilot studies

Equivalent circuit model

Electric circuit equivalent models were developed to describe and understand the properties of our needle electrode setups. Different *in vitro* measurements were done to determine the electrical properties of the needle. From separate measurements of the needle tip (active electrode) and the insulated part of the needle shaft, the properties of these parts of the needle were determined. The most significant properties were modelled by discrete components in the equivalent circuit showed in fig. 11.

Based on the ease of using only one component (CPE) and the nice fit to our data, we here used the model *iv)* in sec. 1.7 to estimate the EPI in this equivalent circuit. The resistance R_E was connected in series with this CPE and together these components modelled the non-insulated active electrode area and its constrictive zone. The values of these equivalents were estimated from measurements keeping only the non-insulated this part of the needle in contact with the saline.

The resistor R_B is given by the resistance in the bulk saline in the used saline tank. The branch containing C_T and R_T models the current path through the Teflon insulation of the needles and the constrictive zone around the shaft. The value of these elements was estimated from the following measurement. The needle tip was inserted all the way through a specially made saline tank keeping the non-insulated tip dry in the air on the distal side of the tank. The tank was then filled with saline to obtain an electrical contact with the Teflon insulated shaft. The tank was equipped with current carrying- and reference electrodes, and a 3-electrode frequency sweep was measured for different lengths of the Teflon insulated section in contact with the saline. From this we obtained capacitance and resistance values as functions of section length and could estimate the impedance as a function of insertion depth.

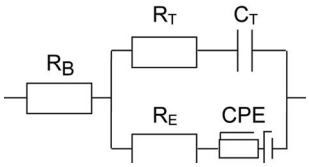

Figure 11: Equivalent model describing the main electrical properties of a needle electrode setup.

The saline used in the *in vitro* experiments is purely resistive at our frequencies (Cooper 1946), and the resistance (R) for a homogenous sample with resistivity ρ, cross sectional area, A, and length, l, is in principle given by the following equation:

$$R = \rho \frac{l}{A} \qquad [\Omega]$$

Eq. 6

The resistance of a homogenous volume can in general be found by converting the l and A in eq. 6 to suited infinitesimal volumes and integrate the resistance over the volume of interest. The estimates of R_B, R_E and R_T based on the measurement were tuned by comparing to this type of analytical calculation. The last step in the model development was done by curve fitting in the Zview software. Differences in component values needed to utilize the model for the different needle types were adjusted by drawing the equivalent model (fig. 11) into the equivalent model library in the Zview model fitting application. A reasonable fit to experimental data was obtained and the model proved was very valuable during the interpretation of our results.

Gold standard comparison

To verify our measurements and the sampling site, we needed a technique to determine the position of the needle tip for each measurement, or to be more exact: the type of tissue in the closest vicinities of the active electrode on the tip of the needles. In laboratory tests impedance was measured in pieces of bacon from the local grocery store. By inserting the needles in defined depths and cutting the bacon along the plane of insertion, the tissue type of the sample site was visually determined based on insertion path and depth. In clinical measurement or in porcine model *in vivo* this procedure is not appropriate. A search among the methods described in sec. 1.2 was done to find a usable "Gold standard" for comparison with our measurement results.

MRI

Bacon was also used as test piece in MRI for determination of the position of a needle. Different types of scans were taken of the bacon with a needle inserted. The test was done with special MRI compatible needles and ordinary medical stainless steel needles e.g. both needle types used in Paper I. Among the tested needles only the MRI compatible needles gave a reasonable image quality. The medical grade stainless steel could not be seen in the obtained image, but the most trouble was caused by the ferromagnetic properties of the needles that distorted the image. Similar distortion was found both in the T1 and GRE scans. A typical example is seen in fig. 12 where an image of a medical stainless steel needle is compared to a MRI compatible needle.

The assortment of MRI compatible needles is quite narrow and we did not found any compatible insulated needle electrodes suited to our application. The large instrumentation, the long scan time and the need to move the Solartron and other measurement equipment out of the room during the imaging process makes this modality rather impractical. Based on these drawbacks and to avoid the complex process of producing special designed MRI compatible electrodes, we decided to try other methods to determine the position of the needles during the impedance measurements.

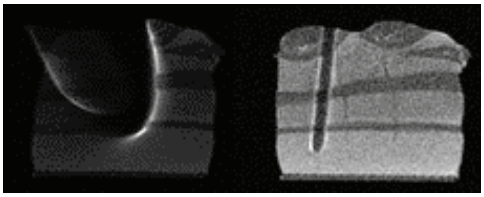

Figure 12: MRI image of bacon distorted by a medical stainless steel electrode (left), and similar placement of MRI compatible in the same piece of bacon (right).

CT

CT and other X-ray modalities gives sufficient contrast between fat, muscle and blood for discrimition of these tissue types. Needles are nicely displayed in CT images and in principle the modality is well suited as a standard for compartion during our measurements. Drawbacks are the exposure to ionizing radiation and that the large and expesive equipment is not readily available. In addition small gantries are inconvinient for some insertion procedures. In combination with the large volume of the total equipment, the gantry will require additional length on the measurement cables. Even if shielded cables are used, increased cable length can interfere with the measurent by introducing additional inductance in the setup. The radiation is not a concern for the porcine *in vivo* models, but in many procedures the operators will also be expoced, especially in dymamic measurements where needle insertions and measurements have to be done with live images.

US
US provides sufficient contrast for discrimination of fat, muscle, blood and nerves. Portable instrumentation is utilizised and only the cable connected transducer probe has to be brought into the direct vicinity of the measurement site. Images are provided relatively quickly with instant exposure, but with some time spent for dynamic location of the needle and tissue.

Both CT and US have properties beneficial for use as a "gold standard" in our experiments. Since the US equipment is portable and handy for use together with our other equipment used during measurements, this modality was preferred compared to the CT that introduces some practical complications and exposure to ionizing radiation.

Electrode contact area hollow needles
In microscope inspections of the needle electrodes we found that the used EMG monopolar needle electrodes had similar insulation leaving the distal conical part of the needle non-insulated, but the hollow needles were found dissimilar. In a closer look at fig. 9 (107x magnification found in Paper III, fig. 8c) we found the Stimuplex A needle to be insulated only on the outside leaving the bevel cut part of the tip and the hollow inside of the needle non-insulated. In a similar inspection of the Stimuplex D we found that the whole visible part of needle, including the tip, was insulated except for a small area on the very tip that seemed to be ground sharp. A thorough inspection of the inside of the hollow part of the needle showed that the insulation did not continue far into the hollow part, but ended approximately at the proximal end of the bevelled tip. Fig. 13 is an illustration of three Stimuplex D needles at different insertion depth in saline. The only visible non-insulated part of the needle is the exposed metal drawn as a dark spot on the very tip, but as explained above there is also a non-insulated area not visible on the inside of the hollow needle. The impedance was measured at three different positions, exposing different areas of the tip to saline; a), the very tip, b), the distal half of the bevel, c), the whole tip to just above the proximal end of the bevel. Repeated measurements in position a) and b) gave insignificant differences in measured impedance spectra, but position c) gave various results. Sometimes only small differences from a) and b) was found, but occasionally a large reduction in impedance for all frequencies was seen. Our suspicion was occasional contact between the saline and the non-insulated inside of the needle. Measurement series done on previously saline filled needles confirmed our suspicion by relatively stable and reduced impedance on all occasions. Based on this finding all hollow needles were filled with saline and the injection tube was cut as short as possible and clogged with a knot before being used in measurements.

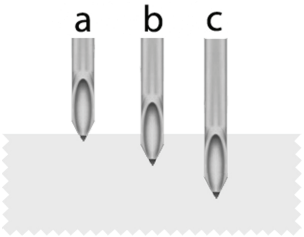

Figure 13: Illustration of Stimuplex D needle electrodes in three different depths into a saline tank

Plastic cannula
The coupling fluid technique explained in section 1.5 and 1.7 D can facilitate venflons or other plastic cannula for use as quasi needle electrodes for stimulation or measurement with reduced influence from EPI or other parasitic behaviour of small electrodes. A prototype was made for a pilot test of this method in our context. The plastic cannula illustrated in fig. 14 (dimensions found in the figure) was made and filled with saline. The whole construction was

made from insulating material except for the saline and the immersed cylindrical aluminium electrode. The expected impedance of the coupling fluid was calculated to 42 kΩ from eq. 6 by insertion of ρ=0.7 Ωm, l=17 mm and A=0.09 mm^2. The measured impedance was slightly higher than this, but found in accordance due to the series resistance in the rest of the coupling fluid and some influence from the electrode properties.

Figure 14: Sketched prototype of a saline filled plastic cannula for impedance measurement.

***In vitro* bacon model**

Pilot tests were done in an *in vitro* bacon model for empirical estimation of spatial sensitivity of our needle electrode setup. Ordinary bacon from the local grocery store was used. Bacon is salted and smoked, but our experience is that because of its distinct lateral separation between fat and muscle it is a well suited model for such experiments.

Preliminary impedance measurements as a function of time were taken with the Solartron setup in "time sweep"-mode. Current carrying and reference electrodes (Blue sensor described in sec. 3.1) were placed on the skin-side of the bacon and the needle electrode (Medtronic 28G, fig. 9) was inserted at constant speed. As the insertion speed was known the time scale could easily be converted to insertion depth. The cross section of the bacon containing the needle path was uncovered by cutting the bacon along the insertion path. Plotting the measured modulus and phase angle as function of insertion dept on a scaled image of the bacon was done to reconstruct the needle's position in the bacon.

As the project went on the needle guidance prototype described later was used in same type of measurements. Fig. 15 shows a measurement done at 3 kHz done with the prototype. Similar results were obtained with the Solartron setup (not shown).

The high spatial resolution of the method is indicated by the abrupt change in the modulus and phase angle in the boundaries between tissue types. Relatively small marbleisation of fat is seen as increased modulus compared to the relatively uniform level in the muscle part of the bacon. A decreased modulus (to muscle level) was found in the subcutaneous fat and some fascias in-between the deeper fat volumes. Another important finding was friction between the needle and the tissue resulted in pushing and pulling forces in the tissue. This was especially pronounced in penetration of fascias, and is seen as a "delay" in the measurement; the change found in the modulus and phase is in some occasions shifted some millimetres to the right compared to the tissue.

The first of these pilot studies was part of the motivation for a further feasibility study and development of the method.

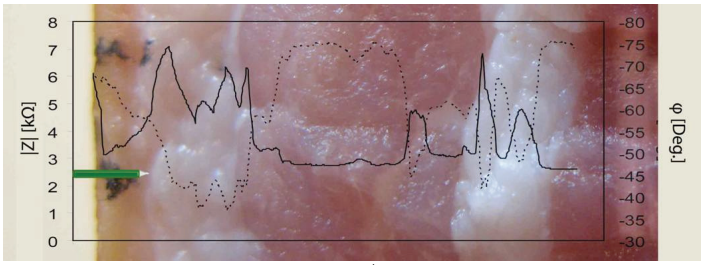

Figure 15: Measured impedance modulus (|Z|) and phase (φ) as a function of insertion depth in bacon (3 kHz). The relation between depth and position in the bacon is illustrated by plotting the measurement on a scaled picture of the bacon.

In vivo model

All *in vivo* measurements on the porcine model were approved by the approved competent person under the surveillance of the Norwegian Animal Research Authority (NARA) and registered by that Authority. A few US guided pilot measurements was also done in blood, muscle and fat on human volunteers. These measurements were in accordance with the results from porcine models.

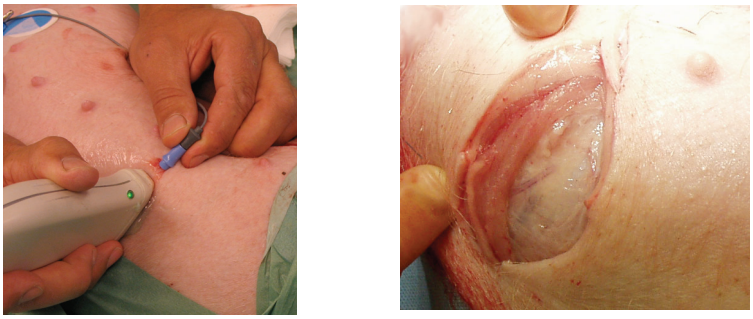

Figure 16: *In vivo* porcine models. Measurement was done with US guidance (left) and by lateral insertion after abdominal incision (right).

Prototype

For obtaining experience as the work was carried out we made a prototype (demonstrator) to test needles and algorithms. The prototype was also used for demonstrating the method for clinicians. Showing the feasibility of the method and ease of use, the demonstrator gave inspiration for new ideas and cooperation in development of future clinical applications. The laptop prototype was based on Labview and a PCMCIA DAQ-card solution from National instrument (Austin, US) and a small front-end electric circuit facilitating 3-electrode measurements. Preliminary discrimination algorithms were developed based on the tissue type specific differences found in the modulus and phase angle measured at 3 kHz and 30 kHz (Paper I). This prototype performed very well in pilot studies on *in vivo* porcine models. For meeting room demonstrations a special software version with algorithms for discrimination between yolk and albumen in boiled eggs, was developed.

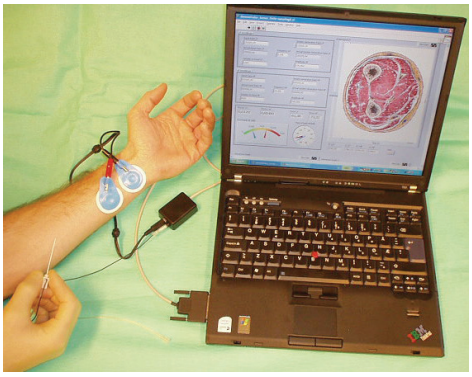

Figure 17: Laptop prototype based on Labview/DAQ-card solution and front-end electronics (small black box on the leads).

4 List of original papers

I. Impedance-based tissue discrimination for needle guidance.
Kalvøy H., Frich L., Grimnes S., Martinsen Ø.G., Hol P.K., Stubhaug A. Physiol. Meas., 30, 129-140, 2009.

II. Current threshold for nerve stimulation depends on electrical impedance of the tissue: A study of ultrasound-guided electrical nerve stimulation of the median nerve.
Sauter A.R., Dodgson M.S., Kalvøy H., Grimnes S., Stubhaug A, Klaastad Ø. Anesth. Analg., 108 (4), 1338-1343, 2009.

III. Electrical impedance of stainless steel needle electrode.
Kalvøy H, Tronstad C, Nordbotten B, Grimnes S, Martinsen ØG,
Annals of biomedical engineering, 2010
DOI : 10.1007/s10439-010-9989-2

IV. New method for separation of electrode polarization impedance from measured tissue impedance.
Kalvøy H, Johnsen GK, Martinsen ØG, Grimnes S
Submitted to IEEE Trans BME, Mars 2010

V. Finite element model of needle electrode spatial sensitivity.
Høyum P, Kalvøy H, Martinsen ØG, Grimnes S
Submitted to Physiol. Meas. March 2010

VI. Invasive electrical impedance tomography for blood vessel detection.
Martinsen ØG, Kalvøy H, Grimnes S, Nordbotten B, Hol PK, Fosse E, Myklebust H, Becker LB
Submitted as short letter to Bentham Open Biomedical Engineering Journal, February 2010

5 Discussion

The discussion is in two sections. The first part contains general considerations applying to the used methods. The second part is the main discussion of the summarised results from all Papers and pilot studies. Results from the individual studies and the discussion of these are found in the reprints of the Papers I-VI.

5.1 General methods

Statistics

To reduce the expense of animal lives and the use of volunteers in invasive procedures the number of repeated measurements have been kept at a minimum at this stage of our project. Through a large amount of pilot testing and measurements in different models (saline, bacon, eggs and other biological materials), we have gained a lot of experience in the fine-tuning of setups and measurements for high quality. Thus, we have reduced the number of animal studies to what we believe is sufficient for showing the feasibility of our methods, and no more. Except for the use of the statistics described in Paper II the number of repeated measurements has not been large enough to facilitate sophisticated statistical analysis.

Temperature

The influence from temperature must be considered in the design of bioimpedance experiments. In general the impedance of a sample is (to some extent) dependent of the temperature, and at the same time the temperature in the sample can be changed by the excitation signal used during the measurement.

Temperature was not logged in the *in vivo* measurements, but in healthy volunteers we presumed a temperature about 36-37 ^{0}C and slightly higher in the *in vivo* porcine models.

To minimize influence from temperature drift (Cooper 1946, Gray and Chandler 2004) in the *in vitro* experiments all measurements and storage of samples and equipment were done in controlled room temperature 23.4 ± 0.7 ^{O}C. A temperature coefficient for saline of 2-3 %/^{O}C, will within this range give an error due to temperature drift of approximately ±2 %. In our context this was not considered significant, but raising the temperature to the *in vivo* level would have caused an estimated temperature drift about ten times higher. Hence, the effects caused by the difference in temperature must be accounted for during interpretations of *in vitro* measurement in a clinical context.

The adiabatic temperature rise per second (ΔT/t) in a sample caused by an excitation current is given by Grimnes and Martinsen 2008 (their eq. 3.43):

$$\frac{\Delta T}{t} = \frac{J^2}{\sigma' c d}$$

Eq. 7

As a typical example we have calculated the temperature change per second (ΔT/t) for three important frequencies using a needle electrode of 0.3 mm^2 in saline. Typical current densities (J) were calculated by using 30 mV excitation voltage, 0.3 mm^2 electrode area and impedance values picked from Paper III. The conductivity of saline (σ'=0.7 m/Ω), the heat capacity (c= 4.2 kJ/kg ^{o}K) and mass density for water (d=1000 kg/m^3) were taken from Grimnes and Martinsen 2008. Typical modulus, corresponding current density and temperature drift per second are listed for three used frequencies in table 2.

Frequency [Hz]	Typical modulus	J [μA/m^2]	ΔT/t [^{0}C/s]
10^6	0.1-1 kΩ	10	$3 \cdot 10^{-2}$
10^4	1 kΩ	3	$3 \cdot 10^{-3}$
1	1 MΩ	0.003	$3 \cdot 10^{-9}$

Table 2: Typical modulus, corresponding current density and temperature drift per second, listed for three different frequencies

The total measurement time for obtaining our spectra was about 100 seconds. From the values in table 2 this corresponds to a hypothetic temperature rise of about 3^0C if we used a 1 MHz measurement frequency. But all our frequency sweeps started at the highest frequencies and were averaged over 6-12 periods for each frequency (some variation between studies). Thus the excitation time was only 6-12 μs at 1 MHz. The length of one period and time spent on averaging is inversely proportional to the frequency. At 1 Hz the measurement time is increased by a factor of 10^6 (6-12 seconds), but at the same time the reduced current density caused by the increased impedance gives a reduction of factor of 10^7 in ΔT/t. Thus, the temperature rise in the samples caused by our excitation current will be much less than one degree and no significant errors can be expected from the temperature coefficient of saline. In tissue *in vivo* even less temperature rise can be expected due to the enhanced heat dispersion caused by the circulation of blood and other body fluids. Fig. 18 shows the pilot result after stimulation with 1 mA in egg white. Coagulation and gas bubbles appeared on the needle electrode surface. A charge transfer way above what we used for excitation was required for bubbles and coagulation to appear.

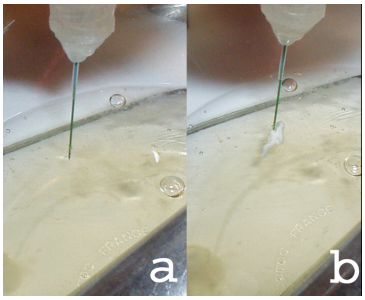

Figure 18: 1 mA DC stimulation of needle electrode in egg white (negative needle).
a: before stimulation, **b:** Resulting coagulation and bubbles in egg white after one minute.

Linear region excitation signal

A 30 mV controlled potential signal was the generally used excitation signal used in our papers. This is well within the linear region (Geddes 1971) for the used electrode sizes from 0.28 mm^2 and above, but we still tested this in the study design of Paper I we tested this in pilot measurements. Measurements with swept amplitude excitation signals were done. According to Geddes' (1971) stainless steel electrode data we expected an amplitude independent range until a certain amplitude where the measured resistance and reactance decreased as the amplitude increased. Our measurements showed that this was not univocally applied to sharp tipped needle electrodes. There was no strictly flat level independent of amplitude. The impedance decreased slightly as the amplitude rose from sub-mV, and the relative decrease increased as the amplitude was increased above 50-100 mV. Our opinion is that this was caused by the uneven current density distribution over the active electrode area due to the sharp tip of the needle. In other words; if the needle is sufficiently sharp there will always be a tiny area on the very tip, which is outside the linear region. The non-linear contribution was kept insignificantly low by not using excitation amplitudes above 30 mV.

5.2 Summarised results

Tissue specific impedance for discrimination *in vivo*

In Paper I, II and VI and pilot studies we measured the impedance *in vivo* in porcine models and human. The results from porcine models are published in Paper I and VI. Repeated measurement with Braun 22G and Medtronic 28G in muscle and fat, and six additional tissue types with the last needle, are plotted in Paper I. Tissue specific frequency sweep was indicated for all eight tissue types, and sufficient characteristic differences for discrimination between fat, muscle and subdermis was found in PCA and PLS analysis. In Paper VI the plotted frequency sweeps done with TECA 28G needle in fat, muscle, artery and vein are plotted and were in accordance with the results from Paper I. Measurements in 26 human volunteers was done in Paper II using the Stimuplex D. This gave a 75 % higher resistance in fat/connective tissue (~35 kΩ) compared to muscle (~20 kΩ). This seems promising for discrimination and is in accordance with the tendency of large modulus found in fat at frequencies above 1 kHz, but further analysis of the resistance values must be done for conclusion. Six complete frequency sweeps in human volunteer pilot tests using TECA 28G needle showed homogenous results for muscle and blood in accordance with the porcine model results, and similar measurement in fat were found partly in accordance with porcine models with occurrences of somewhat higher modulus.

Spatial sensitivity

Finding the optimal spatial sensitivity for use in our applications is not as easy as it might seem at first sight. A common misconception is that the higher the spatial sensitivity the better, but this will in most cases not be true. An illustrative example can be muscle tissue, which needs supply of blood for exchanging of gases and other substances during metabolism. Capillaries and small vessels are found in-between the muscle fibres. Intramuscular fat can also be marbled into a muscle volume. Thus, if the spatial sensitivity is too high we can be mislead by a small fraction of other tissue types. The optimal setup is the one that gives some kind of an average measurement and that reflects the main electrical properties in a sufficiently large volume. The size of the sensitive volume must be evaluated in comparison to the geometry of the tissue compartment we are searching for.
A resolution on the cellular level is not optimal for our applications.

In vitro pilot measurements indicated adequate spatial sensitivity (sec. 3.2), in Paper V the 97% sensitivity radius was calculated to 3.75 mm, in Paper I we showed that the needle tip had to be approached to 2.4 mm from the bottom plate, and the feasibility for blood vessel detection was indicated in Paper VI. All of these applied to 28G needles with active electrode area of approximately 0.3 mm^2. Except for the pilot measurements these results was discussed in the papers and found to be in accordance with each other and the majority of findings published by other investigators.

The Stimuplex D needles (described in detail in sec. 3.2) have significantly smaller active electrode areas and must be presumed to have a sensitivity zone much smaller than described in the previous section. A small electrode area will also have higher influence from EPI. Some frequency sweeps were done with the setup shown in Paper II and preliminary analyzes was done on the results. Our opinion based on these tests was that the combination of large influence from parasitic EPI and very high spatial sensitivity made this needle type less suited for tissue discrimination based on electrical impedance. The intended use of the needles is nerve detection by electric stimulation (ref. sec.1.2). In such a setting the extra high spatial sensitivity is very beneficial, but from our preliminary findings misinterpretations caused by measurements reflecting small inhomogeneities seem more frequent with these needles.

Electrode setup

Measurements and analyses reported in Paper I and V showed that monopolar measurements could be obtained using a sufficiently large indifferent electrode in a 2-electrode setup. The sensitivity zone was found small enough to completely depress the contributions from the indifferent electrode and the bulk tissue outside the constrictive zone, and we found this setup well suited for *in vitro* studies.

Large stainless steel plate indifferent electrode is less convenient for use *in vivo*. From theoretical considerations a 3-electrode setup with a needle measurement electrode should give similar monopolarity. This was confirmed in the pilot tests (e.g. the bacon pilot in sec. 3.2) which gave truly monopolar results. During the *in vivo* measurements the position of the current carrying electrode and the reference electrode was not critical as long as they not were placed in awkward positions intuitively introducing series resistance from narrow tissue regions between the reference and measurement electrode, or was placed very far from the measurement site.

In some applications other electrode configurations obtained by introducing more than one electrode at the needle can probably be beneficial, but in at this stage the focus has been on the enhanced clinical impact likely obtained by using needles already in use in clinics today. In further application development such methods should be explored to optimize the results. Specially designed electrodes can also give commercial benefits by increasing possible income for potential manufacturers or investors.

Stability of electrode properties

During use the electrodes are exposed to different body fluids and tissues. Small direct currents (DC) can also be setup over the electrode interface due to differences in half-cell potential for the different electrodes and non-ideal instrumentation. Changes in electrode properties after exposure to -1 μA was found in Paper I, and exposures of both these types were investigated for five electrode types in Paper III. A current of ± 1 μA DC was used and the exposure to ionic solutions was modelled by saline. This is a simple model compared to tissue and body fluids which contains a large range of different ions and substances not found in saline, but as a first approach we found this model beneficial and large differences between electrode types with similar specifications was found (for details se Paper III). Based on this Paper the TECA 28G needle was best suited for use in the first application for vessel detection described in Paper VI. Further studies to confirm the findings in Paper III in solutions more equal to tissue containing protein and other ions should be done in future studies.

As described above the TECA 28G was best suited for our application, but the summarised results from or monopolar needle electrode measurement gave promising results for feasibility of tissue discrimination and needle guidance for all five needle electrodes in fig. 9. Not all were used in feasibility studies, but from size and other characteristics they should be within a feasible range. As discussed earlier the needle type used in Paper II and illustrated in fig.13, had a very large influence from parasitic EPI and probably to small spatial sensitivity zone. This is why this type not was included for further study.

Parasitic electrode polarization impedance (EPI)

One of the largest challenges using needle electrodes with sub-mm^2 active electrode area is the parasitic EPI. The EPI is dominating a considerable range of our measurement frequencies (below 1 MHz). Paper I indicates that the EPI is modulated by tissue specific properties and most probably the EPI dominated range can give beneficial contribution in discrimination algorithms. Established methods for reducing the influence from EPI or to subtract the EPI from the measurement data is listed in sec. 1.7. In Paper IV we defined a new method for

separation of EPI and tissue data. For optimal performance in future discrimination algorithms, the development of these should be done after data analysis of data both containing the EPI and after subtraction of the EPI.

Equivalent model and simulations
The equivalent circuit model described in sec. 3.2 was used as a basis for understanding the main electrical properties of our needle electrode setups. This was also used to develop the FE-model in Paper V. The spatial sensitivity for one of our needles was estimated from simulations on this model and found to be in accordance with *in vitro* measurement data. Another use of such a model can be simulations in different models of tissue. Based on published impedance data from other investigators (Gabriel *et al.* 1996,) and own tissue measurements, our goal is to develop FE-models for tissues for use in combination with the needle model. We see this as a future tool for use in application development and to estimate results during the design of new studies.

Needle guidance applications
The current work has proven the feasibility of tissue discrimination in small volumes and how this can be used to tell in which tissue type a needle tip is situated (Paper I and VI). In a number of clinical situations this information will be sufficient to proceed with a procedure, which in principle can be made fully automatic for used by an operator with minimal education or training. Examples can be a “green light” for a diabetic patient intending to insert drugs in adipose tissue or similar situations for intramuscular injections. In other situations the user must add knowledge or provide information of anatomy to plan further actions. Applications can probably be both for use in advanced clinical procedures with very high requirements for specially educated personnel and additional advanced operating room instrumentation, but also fully automated procedures as described in paper VI which can be used on the sidewalk in acute medicine. In the present work we have focused on gathering fundamental knowledge and to show the feasibility of the method. A functional prototype for discrimination of fat, muscle and blood in porcine *in vivo* is already built, but further work should be done for better understanding the fundamental properties of the needle electrodes and to secure reliability over time for the method. By the future directions described in sec. 7 we hope to utilise more sophisticated applications.

6 Conclusions

Based on the presented papers and the summarised experience from this project we have concluded that needle guidance based on electrical impedance measurements is feasible, and that further studies and development of the method most probably will be beneficial in clinical use. Fundamental knowledge of electrode electrical properties and parasitic elements was obtained, and a simulation model was developed as a tool for further development of the method. A suited spatial sensitivity zone was obtained using commercially available needle electrodes approved for medical use.

Conclusions for each separate paper are found in the reprints of the Paper I-VI.

7 Future directions

Our conclusions point in the direction of further studies and development of clinical applications.

The first step in this direction is to gather more *in vivo* measurement data from porcine models and human tissue, for use in numerical analysis (described in sec. 1.4) for development of efficient and reliable discrimination algorithms. Algorithm development as a follow-up to the vessel location application in Paper VI is a natural step, but epidural and spinal insertion guidance in animal models are also planned.

One experience from this project is that the fundamental properties of small electrodes have not previously been sufficiently explored. In the present work we pointed out some properties crucial for the long-term stability of the used needle electrodes, but in our opinion there is a large area of unexplained elements with significant influence on the electrode behaviour and measurement results.

In our opinion the most interesting of these elements as a topic for further study is the roughness and shape of the active electrode area. The shape of the electrode surface influences the current density distribution on the surface. Sharp edges as found on the tip of needle electrodes will have enhanced current density compared to other parts of the active area. Liu (1985) and others have investigated roughness and fractal dimensions, but by including how the current density is distributed over a surface, these models could probably be refined.

In our hollow needle measurements we also found a phase angle significantly different from the massif needles (Paper I). A possible explanation can be that the needle inside is a non-insulated contributor to the active area. The relation between shape and electric properties of electrodes in general, including both hollow and sharp elements, should be an interesting topic for many scientists. A quantified measurement of electrode surface roughness can be obtained by atomic force microscope, and we hope to initiate studies of this kind in near future.

Fundamental knowledge of suited electrode properties will be a necessary step for design of optimal electrodes for future applications.

Detection of abnormal or unhealthy tissue is a widely discussed issue in the context of bioimpedance. If applicable needle guidance instruments are developed, including such types of algorithms it will most likely enhance the impact in clinical use. The feasibility of such algorithms has not been an issue in the present work.

This work has been performed at the Rikshospitalet, Oslo University Hospital, which is a highly specialised hospital with national responsibilities within complicated treatments. In our opinion a close relation to clinicians and lab facilities situated within a highly specialized clinical environment has been a great advantage in the work so far and this will probably be even more important in the future work during the development of specialized clinical applications.

8 Appendix

General definitions:

I	– Current	[A]
U	– Potential	[V]
ρ	– Resistivity	[Ωm]
t	– Time	[s]
f	– Current	[Hz]
ω	– Angular freq. (2πf)	[Hz]
R	– Resistance	[Ω]
X	– Reactance	[Ω]
C	– Capacitance	[F]
G	– Conductance	[S] = [Ω^{-1}]
B	– Susceptance	[S]
j	– Imaginary unit	$j = \sqrt{-1}$

Definitions related to impedance model (Z):

$$Z = \frac{U}{I} \qquad [\Omega]$$

$$Z = R + jX$$

$$X = -\frac{1}{\omega C}$$

$$|Z| = \sqrt{R^2 + X^2}$$

$$Z = |Z| e^{j\varphi}$$

$$\varphi = \arctan\frac{X}{R}$$

Definitions related to admittance (Y):

$$Y = \frac{I}{U} = Z^{-1} \qquad [S]$$

$$Y = G + jB$$

$$B = \omega C$$

$$|Y| = \sqrt{G^2 + B^2}$$

$$Y = |Y| e^{j\varphi}$$

$$\varphi = \arctan\frac{B}{G}$$

References:

Abolhassani N, Patel R, (2006) Moallem M, Needle insertion into soft tissue: A survey, Medical Engineering & Physics **29** 413–431

Bordi F, Cametti C and Gili T (2001) Reduction of the contribution of electrode polarization effects in the radiowave dielectric measurements of highly conductive biological cell suspensions, Bioelectrochem. **54** 53-61

Brown BH (2003) Electrical impedance tomography (EIT): a review, J. Med. Eng. Technol. **27** 97-108

Cole KS (1940) Permeability and impermeability of cell membranes for ions. *Cold Spring Harbor Sympos Quant Biol* **8** 110-122

Cole KS and Cole RH (1941) Dispersion and absorption in dielectrics. I. Alternating current characteristics, J. Chem.Pys **9** 341-351

Cooper R (1946) The electrical properties of salt-water solutions over the frequency range 1-400 Mc/s, *J inst Elect Eng* **93** 69-75

Dalrymple P, Chelliah S (2006) Electrical nerve locators, Continuing Education in Anaesthesia, Critical Care & Pain **6** 32-36

Davey CL, Markx GH and Kell DB (1990) Substitution and spreadsheet methods for analysing dielectric spectra of biological systems, Eur. Biophys. J. **18** 255-265

Fricke H (1932) The theory of electrolytic polarization, *Phil. Mag*. **14** 310-318

Gabriel S, Lau R W and Gabriel C (1996) The dielectric properties of biological tissues: II. Measurement in the frequency range 10 Hz to 20 GHz Phys. Med. Biol. **41** 2251–69

Geddes LA, Da Costa CP and Wise G (1971) The impedance of stainless steel electrodes, Med. Biol. Eng. **9** 511–521

Gordon MPJ and Chandler NP (2004) Review: electronic apex locators *Int. Endod. J*. **37** 425–437

Gray JR (2004) *Environment Instrumentation and analysis handbook*, edited by R.D. Down and J.H. Lehr, Wiely 491-510

Grimnes S (1983) Impedance measurement of individual skin surface electrodes. Med. Biol. Eng. Comput. **21** 750-755

Grimnes S and Martinsen ØG (2005) Cole electrical impedance model - a critique and an alternative *IEEE Trans. Biomed. Eng*. **52** 132-135

Grimnes S and Martinsen ØG (2007) Sources of error in tetrapolar impedance measurements on biomaterials and other ionic conductors, J. Physics D: Applied Physics **40** 9-14

Grimnes S and Martinsen ØG (2008) *Bioimpedance and Bioelectricity Basics* 2nd edn (San Diego: Academic)

Khambete N D, Shashidhara J, Bhuvaneshwar GS and Sivakumar R (1995) Impedance measurement system for concentric needle electrodes Proc. RC IEEE-EMBS and 14th. 1.1–1.2

King JC, Dumitru D, Stegeman D (1996) Monopoar needle electrode spatial recording characteristics, Muscle & Nerve **19** 1310-1319

Liu SH (1985) Fractal model for the ac Response for a Rough Interface, Phys. Rev. Letters **55** 529-532

McAdams ET, Lackermeier A, McLaughlin JA, Macken D and Jossinet J (1995) The linear and non-linear electrical properties of the electrode-electrolyte interface, Biosens. Bioelec. **10** 67-74

Mirtahei P, Grimnes S and Martinsen ØG (2005) Electrode Polarization Impedance in Weak NaCl Aqueous Solutions, IEEE Trans. BME **52** 2093-2099

Raicu V, Saibara T and Irimajiri A (1998) Dielectric properties of rat liver in vivo: a noninvasive approach using an open-ended coaxial probe at audior/radio frequencies, Bioelectrochem. Bioener. **47** 325-332

Riu PJ and Lapaz C (1999) Practical limits of the Kramers-Kronig relationship applied to experimental bioimpedance data, Ann. NY Acad. of Sci. 374-380

Riu PJ (2004) Comments on ''Bioelectrical Parameters of the Whole Human Body Obtained Through Bioelectrical Impedance Analysis'', Bioelectromagnetics **25**, 69-71

Scharfetter H, Casañas R and Rosell J (2003) Biological tissue characterization by magnetic induction spectroscopy (MIS): Requirements and limitations, IEEE Trans. BME **50** 870-880

Schwan HP and Li K (1953) Capacity and Conductivity of Body Tissues at Ultrahigh Frequencies, Proc. IRE 1735-1740

Schwan HP (1966) Alternating Current Electrode Polarization, Biophysik **3** 181-201

Schwan HP and Ferris CD (1968) Four electrode null techniques, Rev. Sci. Instrum. **39** 481-485

Schwan HP (1992) Linear and Nonlinear Electrode Polarization and Biological Materials, Ann. Biomed. Eng. **20** 269-288

Stoneman MR, Kosempa M, Gregory WD, Gregory CW, Marx JJ, Mikkelson W, Tjoe J and Raicu V (2007) Correction of electrode polarization contributions to the dielectric properties of normal and canserous breast tissues at audio/radiofrequencies, Phys. Med. biol. **52** 6589-6604

Ulbert I, Halgren E, Heit G and Karmos G (2001) Multiple microelectrode-recording system for human intracortical applications, J. Neurosci Methods. **106** 69-79

I

II

III

IV

New method for separation of electrode polarization impedance from measured tissue impedance

Håvard Kalvøy, Gorm K. Johnsen, Øjan G. Martinsen and Sverre Grimnes

Abstract - **In this paper we have shown that electrode polarization impedance (EPI) can be separated from measured tissue impedance as long as the characteristic frequencies of EPI and tissue are not too close, so that the EPI is largely displayed as a separate dispersion. In 2-electrode measurements the EPI and sample are physically connected in series, and commonly modelled by equivalent components in series. We have calculated the parallel equivalent elements and converted the series connected EPI and sample to a parallel admittance model. By curve fitting on the converted model we have shown that this provides a new method for estimating the EPI with enhanced accuracy compared to similar techniques used on the impedance model**.

Index terms – **Admittance model, Cole-element, curve fitting, multiple dispersions**

I. INTRODUCTION

By converting the impedance values from the series connected sample and electrode polarization impedance (EPI) to a parallel admittance model we have introduced a new method for estimation of the EPI contribution in a set of measurement data.

EPI is a common problem in low frequency electrical bioimpedance measurements [1]-[12] and probably one of the mostly discussed topics in these types of investigations.

The EPI becomes more pronounced in highly conductive media [1][2][6] or when using small electrodes [1]. In Kalvøy *et al.* we even found influence from EPI above 100 kHz in measurements on sub-mm^2 needle electrodes [4]. Together with the dependency of frequency and electrode properties like material [5], radius [1] and shape [18], the EPI has also been shown to be dependent on the measured sample [1][5][6] and current density [1]. Due to the influence from this variety of factors the EPI is not easily separated from the sample properties in an impedance measurement.

Schwan [1] résumés the history of the EPI research since it was first described over a century ago. Among others he refers to different models for describing the behaviour of the EPI. The most common models are:

i) A frequency dependent resistor and capacitor ($R_p(\omega)$ and $C_p(\omega)$) in series [1][7]

ii) A frequency dependent resistor and capacitor in parallel [8]

iii) A Cole circuit or similar [1][17]

iv) Constant Phase Element (CPE)[6][9] [10]

v) A permittivity model similar to the Cole-Cole equation [1][8]

All of these are expected to be connected in series with the sample under investigation.

Different techniques for reduction or correction of the EPI influence on impedance measurement have been proposed over the years. Schwan [1] tabulates seven of these methods. We have listed an expanded version of his table including references to examples and descriptions in Table 1.

Method:	Description:	Used and explained by:
A. Mathematical subtraction	Estimate EPI from modelling and subtract from measurement data	[1][5][6][7][10][11]
B. Electrode distance variation	Eliminate homogenous sample contribution by measuring with different distances between the electrodes	[1][12]
C. Substitution method	Sample is substituted with a calibration solution with known properties to estimate the EPI	[1][2][8][10]
D. 4-electrode	Separate electrode pairs for excitation and pick-up eliminate current in the pick-up electrodes and the EPI is not included in the measurement.	[15][16]
E. Increased current density	Current density above the linear region may reduce the EPI significantly	[1, p 217][12]
F. Electrode modification	Modification of electrode properties for enhanced quality and less EPI	[1][5][10][11]
G. Reduction of sample conductivity	EPI is less pronounced in low conductive media measurements	[1]
H. Electrode-less excitation by magnetic induction	The electrodes and their parasitic properties can be avoided by using a coil and magnetic induction for excitation and measurement.	[9][12]
I. Coupling fluid	The electrodes can be moved out of the current field or be enlarged by using a conductive coupling fluid to establish contact to the sample	[3]

Table 1: Methods for reduction or correction of parasitic electrode properties

Intuitively the best approach is to modify the measurement setup to reduce or eliminate the effect from EPI before measuring. Methods D, F and H are of such a character, and one rule of thumb could be to always consider these methods and evaluate measurement setups in pilot studies before resources are used on further collection of data. Probably because method H has limited relevance for other samples than suspensions, method D and F are the most used among these three. Except for method A, D and F, the other methods need special arrangements or have other limitations that often make them inadequate in the clinic and measurements *in vivo*. Since some applications need special electrode arrangement and the sensitivity and spatial resolution of the measurements are dependent of the electrode setup, method D and F are not always feasible, and many investigators end up with method A and the challenging task of subtracting the EPI from their sample data.

Before extracting the sample data from the measurement results, a thorough understanding of the measurement system and the main factors contributing to the result must be obtained. The need to establish a proper equivalent circuit is almost indisputable. Examples of EPI-models are found above; i) – v). Brodi *et al.* [6] argue for the CPE as a more realistic model of the EPI than $C_p(w) - R_p(w)$. Raicu *et al.* [7] and Stoneman *et al*.[10] use a CPE alone as model to reduce the number of elements that describe the EPI. As discussed above these

models can, if properly fitted to measurement data, be given similar properties at most frequencies, but at DC they fail as realistic models.

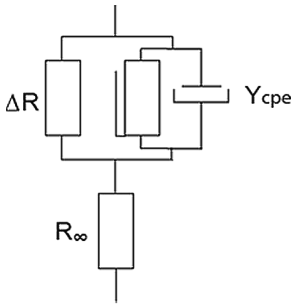

Figure 1. The Cole circuit are commonly used as a electrical model to describe typical EPI properties (Grimnes & Martinsen 2008)

A more general model including DC conductance is obtained by adding a resistance (ΔR) in parallel with the CPE. In modelling measurement data an impedance in series (R_∞) with the CPE is needed to avoid a decrease towards an unrealistic zero impedance as frequency increases. Cole [17] developed his empirical model from fitting to a large series of measurements, and it has since been widely used as a more general model for a single-dispersion system.

In principle a Cole-Cole (permittivity) model [19] could also describe the EPI, but the lack of DC-conductance makes this model less suited than the Cole model. By combining the circuit in Figure 1 with an electric model of the measured object connected in series (e.g. fig. 2), we have a very general model able to simulate the behaviour of most measuring setups. As a general approach we here used a system with two dispersions simulated with two Cole elements in series (fig. 2). In principle a method suited to separate two dispersions can also be used to separate dispersions one by one in a more complex system with multiple dispersions.

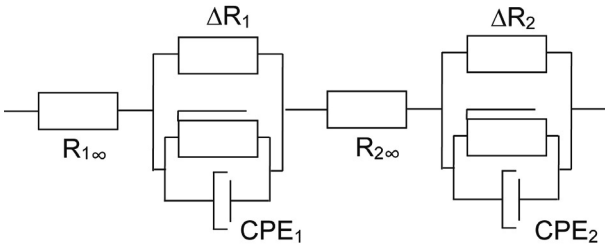

Figure 2: Two Cole elements in series used to simulate a system with two dispersions. All components in the left Cole element have subscription e, and were used to model the behaviour of the electrode interface (EPI). The right Cole element, with subscript t, was given values to represent the sample.

$$Z_{tot} = R_\infty + \frac{\Delta R_1}{1 + (j\omega\tau_1)^{\alpha_1}} + \frac{\Delta R_2}{1 + (j\omega\tau_2)^{\alpha_2}}$$

$$R_\infty = R_{1\infty} + R_{2\infty}$$

Eq. 1

Reducing the resistances in series to one component will not influence the simulation, and we simplify by setting in Eq.1.

Since we here used a model with two dispersions (Cole elements iii)) in series, a representation in impedance parameters (Eq. 1 and Figure 2) is common. The impedance model parameters are converging towards their smallest modulus at high frequencies. At low frequencies the impedance modulus can become very large or diverge to very high impedance at DC. An admittance model has the opposite characteristics, and converges to a finite modulus at DC. Hence, it seems like a good idea to transform the impedance parameters of the series circuit in Figure 2 to an equivalent admittance model, which does not diverge at the frequencies where the EPI is most dominant. To evaluate a new method to extract tissue and EPI properties from a set of measurement data we have simulated the dispersions of the circuit presented in Figure 2 in this study.

II. Materials and Methods

Simulations

Two Cole elements in series (Figure 2 and Eq. 1) were used as model in mathematical simulations of a general system of two dispersions. Time constants with large differences (τ_1=0.00001 and τ_2=1) and values of the constants in Eq. 1 were chosen to obtain two dispersions without overlap. Impedance Wessel-plots of real and imaginary component of the resulting complex impedance were made for different values of ΔR_1 while the other variables were kept unchanged. Resistances in the range between 0 and 32 Ω were used in the distribution found in fig. 5. Equivalent admittance values were calculated and compared in a similar admittance Wessel-plot with conductance (G) and susceptance (B) values on the axis. The next step was to make similar admittance Wessel-plots for different time constants in one of the CPEs while all resistance values were kept unchanged. This was done by setting τ_2=1and varying τ_1 from 0.00001 to 1000 in steps of one decade.

Theoretical analysis

The impedance of the EPI and measured tissue is given by our model in eq. 1, where each of the Cole elements represents an impedance physically in series. Each of the two elements will, if plotted separately, produce depressed circular arcs in the complex Wessel plane. If two or more elements are in series, the net arc will in general be a superposition of the elements, and differ from the arcs of the separate contributions. However, if the characteristic time constants of each of the elements are sufficiently different, we will retrieve separate dispersions in the Wessel plane, and thus EPI can be subtracted from measurement data without subtracting also data from the tissue under consideration. This can be shown by the following:

Assume that the characteristic time constant of tissue, τ_t, differs substantially from that of the EPI, τ_e (which usually is rather high compared to τ_t), i.e. that $\tau_e >> \tau_t$. The admittance of the two Cole elements is then given by:

$$Y = \frac{1}{Z_{tot}} = \frac{1}{R_{e\infty} + \frac{\Delta R_e}{1 + \left(j\omega\tau_t \frac{\tau_t}{\tau_e} \right)^{\alpha_e}} + R_{t\infty} \frac{\Delta R_t}{1 + \left(j\omega\tau_t \right)^{\alpha_t}}}$$

Eq. 2

If tissue measurements are performed in the frequency range much higher than the characteristic frequency of the EPI, and where the measurement frequency is of the order of $(2\pi\tau_t)^{-1}$ the admittance then is:

$$Y \approx \frac{1}{R_{t\infty} + \frac{\Delta R_t}{1 + \left(j\omega\tau_t \right)^{\alpha_t}}}$$

Eq. 3

Where we now have assumed $R_{t\infty} >> R_{e\infty}$, meaning that the EPI at very high frequencies can be neglected compared to the corresponding tissue impedance. This assumption is reasonable, and has earlier been shown among others in studies of EPI [5][11, p 266] as well as in electrode modelling where the EPI is modelled so that one of the branches in the equivalent circuit is a capacitor alone, resulting in a shunt at high frequencies [11,p 50]. As the double layer between electrode and tissue is very thin, the capacitance in the EPI equivalent circuit will be very large which further reduces the influence of $R_{e\infty}$.

Thus, it is clear that characteristic tissue impedance data can, under the conditions described above, be found by fitting measurement data to one single Cole element without influence from EPI, or to state it differently: as if the EPI was not at all present.

Model measurements

The EPI-correction method was tested in practice by doing measurements on a cucumber. A comparison to the simulated data was obtained by selection of a one

dispersion sample influenced by EPI. Cucumbers display one distinct dispersion with a characteristic frequency around 50 kHz and are easy to handle as a measurement object. A fresh cucumber was cut to 60 mm length. The plastic wrapping was kept on the long side to avoid the cucumber to dry out during the measurements.

Figure 3: 2-electrode measurement setup showing cucumber (60 mm), stainless steel electrodes (50 mm x 65 mm), weight (500 g) and connection leads.

The cucumber was placed upright on the table with a stainless steel plate electrode (50 x 65 mm) covering the cross section on each end. A 500 grams weight was placed on top of the upper electrode plate to provide a firm pressure and secure stable contact at the electrode interfaces. A Solarton 1260/1294 impedance measurement system was connected in the 2-electrode setup shown in Figure 3 and frequency sweeps from 10 mHz to 1 MHz were done with a controlled potential of 30 mV rms.

The electrodes were given three different treatments to obtain different influence from EPI in the measurements. First sweep was with dry electrodes, the second was with saline (NaCl 0.9%) wetted electrodes and the third was after a firm wipe of silicone high vacuum grease on the electrode surface.

III. Results

Simulations

The simulations based on our model in eq. 1 gave two circular segments in the Wessel-plots as expected. For the impedance model in Figure 4 the HF dispersion became an almost complete segment ending near the real axis on both sides. The LF segment tended to diverge to very high values for the lowest frequencies as the ΔR_1 increased. Very low simulation frequencies had to be used to determine the circular shape. We also note that the simulations produce two separate arcs as the characteristic time constants of the EPI and tissue impedance are very different.

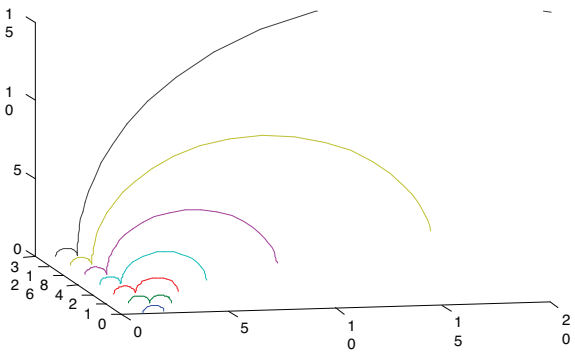

Figure 4: Impedance model Wessel-plot of two dispersions plotted for different ΔR_1.

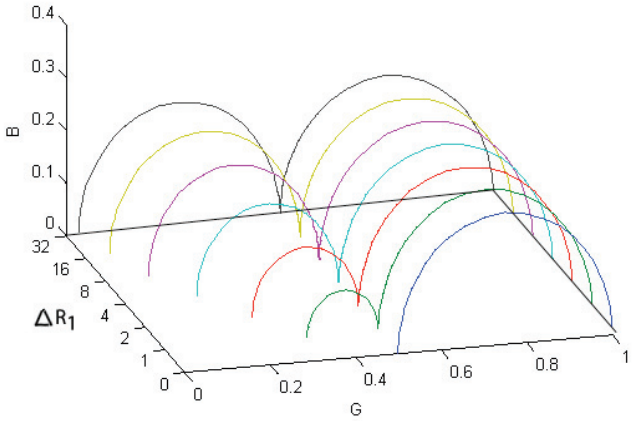

Figure 5: Admittance model Wessel-plot of two dispersions for different ΔR_1

For the admittance model plotted in Figure 5 both dispersions gave almost complete segments ending close to the real axis, and as the ΔR_1 increased the admittance converged towards zero at the lowest frequencies. Both dispersions could easily be fitted to a Cole segment, and subtraction of a parasitic LF can be done with enhanced precision in this model compared to the same data plotted in the impedance model (Figure 4).

Data in Figure 4 and Figure 5 were simulated with time constants τ_2=1 and τ_1=0.00001 resulting in a 5 decades difference. The resultant admittance Wessel-plot for different values of τ_1 is illustrated in Figure 6 (all other values unchanged).

The dispersions melt together as the time constants become equal. Davey *et al.* [8] also showed this in their fig. 8, which corresponded to a -1 decade in time constant (purple line).

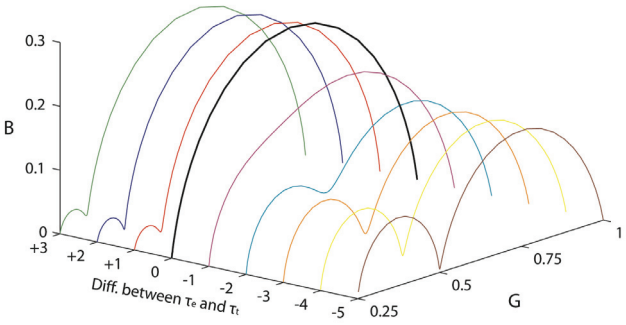

Figure 6: Admittance Wessel-plot for different values of τ_1.

Example measurements

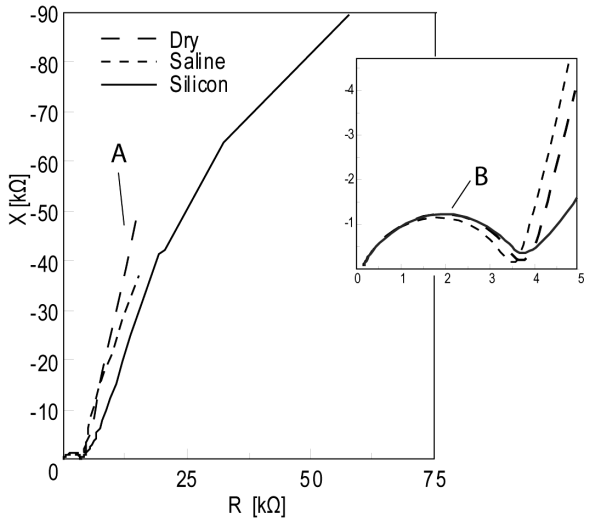

Figure 7: Impedance model Wessel-plot of *in vitro* measurement data. Segment **A**: EPI, Segment **B**: Sample. Details from the HF tail inserted.

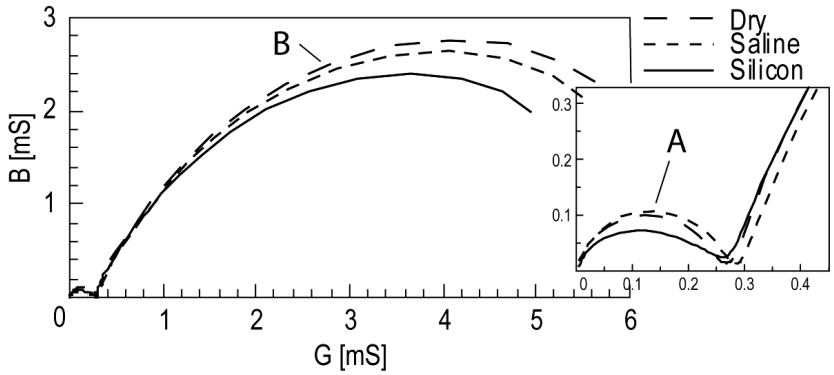

Figure 8: Admittance model Wessel-plot of *in vitro* measurement data. Segment **A**: EPI, Segment **B**: Sample. Details from the LF tail inserted.

The results from the *in vitro* model measurements are plotted in Figure 7 and Figure 8. The LF segment (A) corresponding to the EPI was not possible to estimate by curve fitting to a Cole element with high accuracy in the impedance model Wessel-plot. In the admittance model Wessel-plot nearly complete arcs of circular segments were found for the A segment.

IV. Discussion

In this paper we have shown, analytically as well as experimentally, that EPI can be separated from tissue measurements as long as the characteristic frequencies of tissue and EPI are not too close, so that the EPI is given as a separate dispersion in the Wessel plane.

EPI is a poorly controllable parasitic element with various properties. Small changes in contact area, humidity, roughness or treatment of the electrode interface can give large variations between measurements. The cucumber model has a β-dispersion in about the same frequency range as found in muscle tissue *in vivo* [13], and a relatively frequency independent modulus and low phase angle at LF. The rigid structure and stable electric properties over time makes it very suitable as a model for reproducible measurement. By using a stable sample and three different preparations of the electrode surface, we aimed for a setup where all variations in the measurement data were caused by the variations in electrode properties causing the EPI. From interpretation of the simulations and analysis we expected the B segments in figure 7 and 8 to be close to identical for all three measurements. Since the admittance decreased for each measurement, the *in vitro* results were not in complete accordance with the expected. Since the admittance decreased chronologically and each measurement took about 50 minutes our guess is that the cucumber was affected by the storage in room temperature, and that drying of the cucumber between each measurement caused the decreased admittance.

As seen in the simulation results the LF tail converges towards a small value in the admittance model giving an enhanced accuracy during curve fitting compared to the impedance model. In the *in vitro* data the benefits of the admittance Wessel-plots were even more pronounced. Segment A in the impedance model (figure 7) almost looked like straight lines for the dry and saline wetted electrodes. If curve fitting to a circular arc can be done, the accuracy of the result will probably be very poor. The same data plotted in the admittance model (figure 8) gave almost complete arcs.

The admittance plots for variation in time constant (Figure 6) illustrate the limitation due to similarity of the time constants. As the difference in time constant between the EPI and sample decreases below 2-3 decades the accuracy of our method also decreases. This is in accordance with Raicu *et al.* [7] and Stoneman *et al.* [10] who commented that separation methods will not yield if the measured sample has dispersion in the same frequency range as the EPI. Geometrical considerations should also be done. If one or more of the electrodes are small compared to the tissue surface where they are placed, there will be a constrictive zone in the tissue side of the electrode tissue interface. This constrictive zone will have an enhanced current density compared to the rest of the tissue, resulting in an increased impedance contribution from this volume [11]. Hence, the electrode and tissue geometry will be reflected in the measurement at all frequencies even if the EPI is removed. The electrode plates used in the present measurements were made larger than the cucumber cross section to secure contact over the whole cross section resulting in homogenous current density through the whole sample.

Brodi *et al.* [6] focused on using solely a CPE and used a Cole-Cole plot to fit their suspension data. This can be regarded as a method not far from ours. In our opinion they used a Cole-Cole permittivity model to fit to the measurement data, and through their equations they showed that a CPE can be used to describe their results. They only indirectly used the CPE model, which would have been a straight line through origin in their permittivity plot. Since the difference in method only is the dependency of the frequency through $B=\omega C= \omega\varepsilon k_g$ (where k_g is a geometrical constant measured in meters eg. k_g for a parallel plate capacitor is A/L), their method will have some of the same benefits as ours.

V. Conclusion

Converting impedances connected in series to a parallel admittance model is an effective method for estimation of EPI or other LF properties by curve fitting in Wessel-plots. The divergence towards a low value at LF in the admittance model will in most cases give

an enhanced accuracy compared to a similar technique used on an impedance model. As other methods the accuracy decreases as the separation of time constants of the EPI and dispersions in the sample decreases. The method is only limited by the requirement of at least two decades difference in characteristic time constant needed for separation of the circular elements.

REFERENCES

[1] H.P. Schwan , Linear and Nonlinear Electrode Polarization and Biological Materials, Ann. Biomed. Eng. Vol. 20, pp. 269-288, 1992

[2] S. Gabriel, R.W. Lau and C. Gabriel, The dielectric properties of biological tissues: II. Measurement in the frequency range 10 Hz to 20 GHz Phys. Med. Biol. 41 2251–69, 1996

[3] H. P. Schwan, Biophysik 3, 181, 1966

[4] H. Kalvøy, C. Tronstad, B. Nordbotten, S. Grimnes and Ø.G. Martinsen, Electrical impedance of stainless steel needle electrodes, Ann. Biomed. Eng. 2010 DOI : 10.1007/s10439-010-9989-2

[5] P. Mirtaheri, S. Grimnes and Ø.G. Martinsen, Electrode Polarization Impedance in Weak NaCl Aqueous Solutions, IEEE Trans Biomed Eng, v 52, 12, Des 2005

[6] F. Bordi, C. Cametti, and T. Gili, Reduction of the contribution of electrode polarization effects in the radiowave dielectric measurements of highly conductive biological cell suspensions, Bioelectrochem. 54, 53-61, 2001

[7] V. Raicu, T Saibara and A Irimajiri, Dielectric properties of rat liver in vivo: a noninvasive approach using an open-ended coaxial probe at audior/radio frequencies, Bioelectrochem Bioener 47, 325-332, 1998

[8] C. L. Davey, G. H. Markx, and D. B. Kell, Substitution and spreadsheet methods for analysing dielectric spectra of biological systems, Eur Biophys J 18:255-265, 1990

[9] E.T. McAdams, A. Lackermeier, J.A. McLaughlin, D. Macken and J. Jossinet, The linear and non-linear electrical properties of the electrode-electrolyte interface, Biosens Bioelec 10, 67-74, 1995

[10] M.R. Stoneman, M. Kosempa, W.D. Gregory, C.W. Gregory, J.J. Marx, W. Mikkelson, J. Tjoe and V. Raicu, Correction of electrode polarization contributions to the dielectric properties of normal and cancerous breast tissues at audio/radiofrequencies, Phys Med biol 52, 6589-6604, 2007

[11] S. Grimnes and Ø.G. Martinsen, Bioimpedance & Bioelectricity Basics, Second Edition, San Diego, Academic Press, 2008, 471 pp

[12] L.A. Geddes, C. P. Da Costa and G. Wise, The impedance of stainless steel electrodes, Med. Biol. Eng., vol. 9, pp. 511–521, 1971

[13] H. Kalvøy, L. Frich, S. Grimnes, Ø.G. Martinsen, P.K. Hol and A. Stubbhaug, Impedance based tissue discrimination for needle guidance, Physiol. Meas. 30, 129-140, 2009

[14] H. Scharfetter, R. Casañas, J. Rosell, Biological tissue characterization by magnetic induction spectroscopy (MIS): Requirements and limitations, IEEE Trans BME 50, 7, 2003

[15] H. P. Schwan and C. D. Ferris, Four electrode null techniques Rev. Sci. Instrum. 39, 481, 1968

[16] S. Grimnes and Ø.G. Martinsen, Sources of error in tetrapolar impedance measurements on biomaterials and other ionic conductors, J. Physics D: Applied Physics, 40, 9-14, 2007.

[17] K.S. Cole, Permeability and impermeability of cell membranes for ions. Cold Spring Harbor Sympos Quant Biol 8, 110-122, 1940

[18] S.H. Liu, Fractal model for the ac Response for a Rough Interface, Phys. Rev. Letters 55, 529-532, 1985

[19] K.S. Cole and R.H. Cole, Dispersion and absorption in dielectrics. I. Alternating current characteristics, J. Chem.Pys 9, 341-351,1941

V

Finite element model of needle electrode spatial sensitivity

Per Høyum[1], **Håvard Kalvøy**[2], **Ørjan G. Martinsen**[1,2] **and Sverre Grimnes**[1,2]

1. Department of Physics, University of Oslo, Norway
2. Dept. of Biomedical & Clinical Engineering, Oslo University Hospital, Rikshospitalet, Norway

E-mail: per@hoyum.net

Abstract
We used the Finite Element (FE) Method to estimate the spatial sensitivity of a needle electrode for bioimpedance measurements. This current conducting needle with insulated shaft was inserted in a saline solution and current was measured at the neutral electrode. Model resistance and reactance were calculated and successfully compared with measurements on a laboratory model. The sensitivity field was described graphically based on these FE simulations.

Keywords*:* FEM, needle electrode, electrical polarization impedance (EPI), bioimpedance, stainless steel, spatial sensitivity

1. Introduction

The main objective for this work was to describe the spatial sensitivity field of a needle electrode with an insulated shaft.

Spatial sensitivity is a frequently discussed topic in the field of impedance measurements. A common misconception is that the measurement reflects the properties of the sample situated between the measurement electrodes. In most cases this is not very accurate, and for small electrodes (relative to the tissue volume between them) this can be completely wrong.

Earlier investigators have estimated the spatial sensitivity of monopolar needle electrodes in different ways, (Cao et al. 2002)(Kinouchi et al. 1997) but despite of the high relevance we are not aware of any published models for estimating spatial sensitivity for needle electrodes.

Needle electrodes are widely used in different clinical procedures and a high quality electrical model for better descriptions of needle electrodes will hence be of great value. Typical examples are measurements and stimulations in anaesthesiology and neurology (Tsui et al. 2004) (Sauter et al. 2009)(King et al. 1998)

The goal for this study was to develop a method to describe the sensitivity field for needle electrodes in an ongoing project concerning a new method for anatomical needle positioning in the clinic (Kalvøy et al. 2009). The description of sensitivity field will furthermore be important in an ongoing resuscitation project using bioimpedance measurements to confirm intravascular needle position. The objective of this project is to assure fast and accurate access to blood vessels for administration of drugs and liquid for induced hypothermia.

The sensitivity field S can be expressed by the following equation (Geselowitz 1971):

$$\mathbf{S} = \boldsymbol{J}'_{reci} \cdot \boldsymbol{J}'_{cc} \qquad \text{[Eq.1]}$$

($\boldsymbol{J}'_{cc}$ and $\boldsymbol{J}'_{reci}$ are current density vectors which will be explained in detail in section II)

In the case of a two electrode system, S becomes:

$$S = |\boldsymbol{J}'|^2 \qquad [1/\mathrm{m}^4] \qquad \text{[Eq.2]}$$

To obtain the sensitivity field distribution for this system, a Finite Element (FE) model was used. This FE-model was based on an actual lab-model (Kalvøy et al. 2009) with a needle in saline solution. The saline solution was considered as being purely resistive due to our measuring frequency in the sub megahertz range (Cooper 1946).

The needle was modelled with an insulated shaft. This insulation can be envisaged as a cylindrical capacitor with a capacitance given by the insulation thickness and the inserted length in saline solution. When this non-insulated active electrode surface is brought into contact with biological tissue or an electrolytic solution, different electrochemical phenomena will occur resulting in EPI layer. The EPI was modelled as a constant phase element (CPE) in the equivalent circuit (Mcadams et al.1995). A literature study showed that a description of electrode properties as double layer, faradaic charge transfer and sorption as layers with certain thickness, permittivity and conductivity, was not easily obtained. However, a high quality descriptive model should be feasible without an exact match on the molecular level, and in the present work we have defined all electrode interface properties as an EPI layer.

2. Materials and methods

2.1. The electrical model

To establish a FE-model able to simulate the properties of the needle electrode setup, we first had to determine the main properties of the real setup used in the laboratory. From separate measurements of the different parts of the needle electrode (insulation and active electrode area), and analytical calculations, we found that the equivalent circuit in Figure 1 would adequately describe our setup if the components where properly adjusted. This was verified by curve fitting to frequency spectra measured in-vitro using the setup shown in Kalvøy et al. 2009. This model was used as a design basis for the FE-model and also as a tool to interpret the solutions/results from the FE-model.

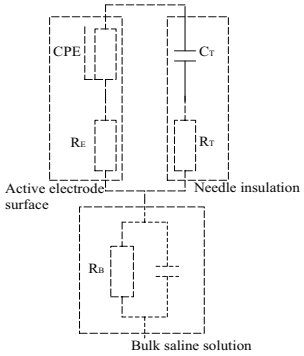

Figure 1. The equivalent circuit used as a simplified electrical model of the measurement setup. The bulk capacitance can be omitted as saline is purely resistive for frequencies up to 600 MHz (Cooper 1946)

As shown above, the electrical model consists of three main parts: the active electrode surface (EPI constructional zone), the needle insulation and the bulk saline solution.

The resistor R_B was used for modeling the bulk saline solution in the tank. This component was used to visualize a change in resistance caused by an increased distance between the bottom plate and the needle without changing the components modeling the needle and its vicinities. Because of the small current density in the large volume of the bulk saline, the resistance of R_B is typically in the order of a few ohms. Thus, changes in this resistance will in most cases be negligible compared to the impedance of the other components, except when the electrode is close to the neutral plate where the total impedance is small.

Multiphysics has no application for implementing CPE directly into a FE-model, but if the frequency is constant a CPE will be reduced to an ideal resistance and capacitance (Grimnes and Martinsen 2008). The simulations in this study were conducted with a single frequency of 100 kHz, and the equivalent conductivity and permittivity were inserted in the FE-model.

The current leaving the active electrode surface will meet the impedance of the saline in the immediate vicinity of the needle tip. An enhanced resistivity is found in this constrictive zone (Grimnes and Martinsen 2008) caused by the relatively high current density in this volume compared to the bulk. The resistance (R_E) in series with the CPE was added to model the purely resistive properties of the saline in this constrictive zone. The CPE is constant regardless of the insertion depth, but with a value given by the geometry and electrical properties of the modeled layer.

The needle insulation can be seen as a cylindrical capacitor with the Teflon insulation as the dielectric. This constitutes a current path in parallel with the CPE which we modeled by C_T. The size of this capacitor will depend on the insertion depth according to the area of insulation exposed to the saline solution. Before entering the bulk the current through C_T must pass the saline in the closest vicinities of the Teflon. Because of the relatively small cross section of this sub-volume, compared to the bulk, an increased resistance is found here. This is implemented in the model by the use of the resistance R_T.

1.2. The geometrical model for finite element simulations

In the following, the structure of the geometrical model template will be described.

This model template was modified for each simulation by repositioning the needle to the specific depth. This resulted in the separate FE-models which are different in only one way; the distance between needle and the saline tank neutral bottom plate.

The resistances R_E, R_T and R_B in Figure 1, model the properties of different volumes of the saline. In a 3D FE-model the input conductivity and the defined geometry will replace these three components. This will enable a much more detailed model (quantified below) and will in most cases give a better match to the laboratory setup measurements.

The saline solution was modelled as a cylinder with height 35 mm and a radius of 52.5 mm. All elements between this cylindrical boundary and the needle were defined as saline (conductivity $\sigma = 1.3$ S/m (Grimnes and Martinsen 2008)).

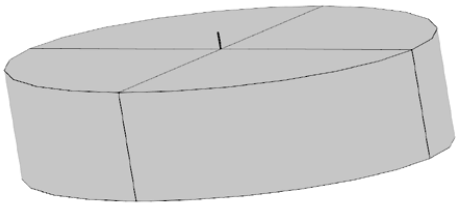

Figure 2. The saline cylinder. The inserted needle is shown in the centre of the cylinder.

The needle “Disposable Monopolar Needle Electrode, 37 x 0.33 mm, Medtronic Inc, Minneapolis, US” has an active electrode area of 0.3 mm^2. This needle has an

insulated shaft. The thickness of this insulation is estimated to 26μm based on our own measurements and information from the manufacturer.

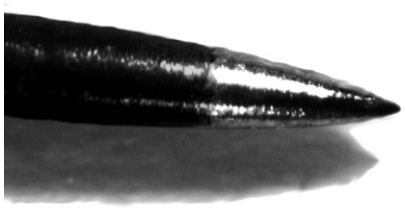

Figure 3. The needle (37 X 0,33 mm)

Metal parts were given a relative permittivity $\varepsilon_r = 1$ and conductivity $\sigma = 4.032 \cdot 10^6$ S/m corresponding to stainless steel. Insulation were given a relative permittivity $\varepsilon_r = 12.1$ and conductivity $\sigma = 1 \cdot 10^{-12}$ S/m corresponding to Teflon

The needle was modelled with a simplification concerning the transition from Teflon insulation to the bare needle tip. This can clearly be seen when figure 5 and 3 are compared: the FE-model has a defined step where there should have been a smooth transition from Teflon to metal. A more accurate transition zone will be subject for further work. Another simplification was to the needle tip curvature and length of the bare metal needle tip. These figures were not given from the manufacturer, and they had to be estimated from visual inspection in a microscope. These estimates, together with the known needle diameter, were tuned to make the correct electrode area (according to the manufacturer). A more accurate needle geometry model will be subject for further work.

The main challenge in modelling the EPI was defining its corresponding geometry and electrical properties. To find the electrical properties, the electrical model was used and compared with the lab measurements conducted by Kalvøy et al. 2009. The EPI geometrical thickness in the FE-model, should of course have been as close to a real thickness as possible, but as described (Grimnes and Martinsen 2008); EPI thickness means small dimensions in the nm range giving an unnecessary complicated FE-model. This resulted in a FE-model with a "suitable" layer thickness of 0.5 μm and with adapted conductivity/permittivity giving the correct values for the CPE; a trade-off between the realistic model and a model that could easily be made and still perform well without reducing accuracy.

EPI was modeled as a layer of 0.5 μm with a relative permittivity (ε_r) of 1000 and conductivity (σ) 0.01 S/m

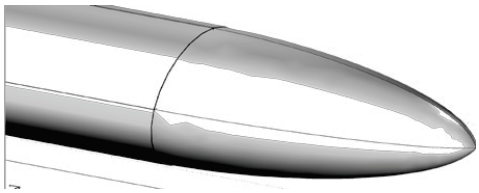

Figure 4. The needle electrode as it has been modelled

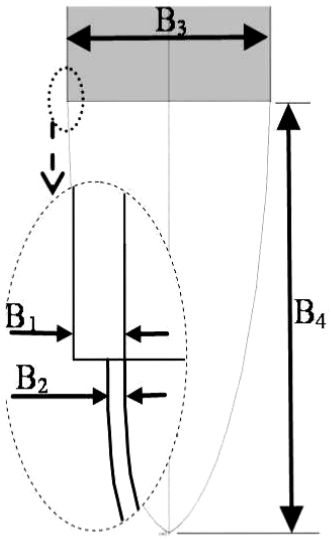

Figure 5. Illustration of the needle tip geometry dimensions (not to scale) B1=26μm B2 = 0.5μm B3 = 0.33mm and B4 =0.4 mm

1.3. The finite element model

To get a 3D FE-model definition of the geometrical model, an axis-symmetrical approach was chosen. This simplified the model to a 2D-definition, which is far easier to simulate and handle than a real 3D-definition. The solutions from an axis-symmetrical 2D-definition will still account for all spatial contributions, i.e. a 3D-solution.

The following boundary conditions (Type A-E defined in Figure 6) were applied to the model. Boundaries being in the centre of the model were treated as axis- symmetrical boundaries (type A). The 2D-model is revolved 360˚ around this axis shown as a dotted vertical line in Figure 6 where the radius = 0. The model had its excitation at the upper needle end with a potential of 1.0 volts applied as an Electric potential

(type B) $V = V_0$ which specifies the voltage at the boundary. Since the wanted solution is a potential, it is necessary to define its value in the geometry for the solution to be valid. Ground (type C) was simply applied as $V = 0$

Electric insulation (type D) was applied as insulation giving $\boldsymbol{n} \cdot \boldsymbol{J} = 0$ specifying that electric displacement is zero outside the boundary. All other interior boundaries were defined as Continuity (type E) where $\boldsymbol{n} \cdot (\boldsymbol{J_1} - \boldsymbol{J_2}) = 0$. This specifies that the normal component of the electric current is continuous across the interior boundary.

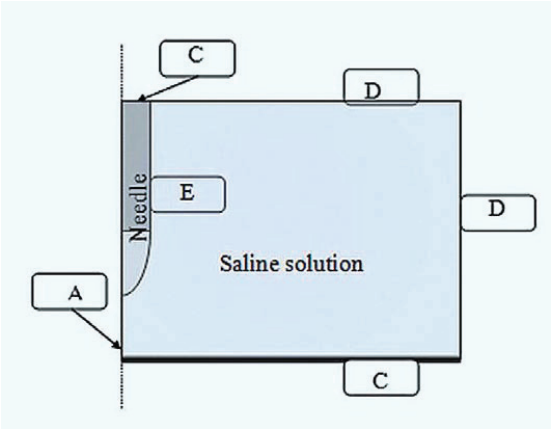

Figure 6. Boundary Conditions for the 2D- model (not to scale)
(Type A-E further explained in the text)

A built-in application mode was used to define the Partial Differential Equations (PDEs); Meriodonal Electrical Currents for Quasi-Static fields. (COMSOL Multiphysics Manual 2008)

$$-\nabla \cdot \mathrm{d}\big((\sigma + \mathrm{j}\omega\varepsilon_0)\nabla V - (\mathbf{J}^{\mathrm{e}} + \mathrm{j}\omega\mathbf{P})\big) = \mathrm{d}\mathbf{Q}_{\mathrm{j}}$$

This has its origin in the Maxwell equations based on the following assumptions being valid:

$$\frac{\partial \boldsymbol{D}}{\partial t} = 0$$

As to the Maxwell equations, changes in time of currents and charges are not synchronized with the changes of the electromagnetic fields. If this effect can be ignored, electromagnetic fields can be described by only considering stationary currents. This approximation is valid when time variations are small and the studied objects are far smaller than the wavelength. The needle model frequency is 100 kHz and largest model part 50 millimetres. This shows that this FE-model can be defined and solved as a Quasi-Static field.

The skin depth in all domains is much larger than the geometry, resulting in an approximation that neglects the coupling between the electric and the magnetic fields, giving:

$$\nabla \times \mathbf{E} = \mathbf{0}$$

Meshing of the model has been done by using the straight forward method given by the meshing routines in CM, only based on model geometry. The mesh could have been optimized with a lesser number of elements and probably become a more efficient model concerning the usage of computer force, but due to the choice of using an Axis-symmetric approach, all solving/handling of the model has been made easier.

To verify the FE-model element minimum quality (q), we used to following simple equation:

$$q = \frac{4\sqrt{3}A}{h_1^2+h_2^2+h_3^2} \qquad \text{[Eq.4]}$$

Where A is the triangle area and h_1, h_2 and h_3 are the side lengths of the triangular element. If q > 0.3 the mesh quality should not affect the solution quality. (COMSOL Multiphysics Manual 2008) We found that q was equal to 0.46 and hence, an acceptable element quality.

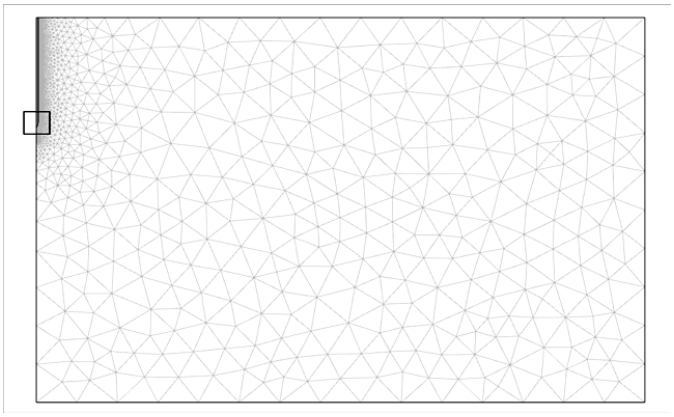

Figure 7. The complete model. The needle tip is marked with a square. The contents of this square can be seen in Figure 8.

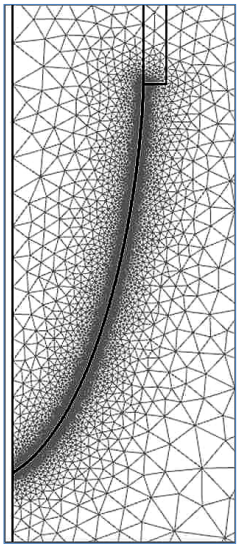

Figure 8. Magnified section of the mesh from the proximity of the needle (see figure 7)

The application (CM) will normally select the appropriate solver for the FE-model. This was also true for this model and a thorough discussion of the choice of solver is therefore left out. A linear system solver called Direct (SPOOLES) was used. For further information about CM solvers, see (COMSOL Multiphysics Manual 2008).

1.4. Sensitivity

The measured potential between the needle tip and the neutral plate can be described by:

$$u = \iiint \rho \, \boldsymbol{J}_{reci} \cdot \boldsymbol{J}_{cc} \, dV$$

If we define

$$\boldsymbol{J}' = \frac{\boldsymbol{J}}{\boldsymbol{I}_{reci}}$$

where $\boldsymbol{I}_{reci}$ is the current in the needle. Then we get $\boldsymbol{J}'$ as a unity current density. We can express the system transfer impedance with

$$Z = \iiint \rho \, \boldsymbol{J}'_{reci} \cdot \boldsymbol{J}'_{cc} \, dV \qquad \text{[Eq. 5]}$$

The spatial distribution of S ([Eq.1] and [Eq.2]) gives the sensitivity field, and by multiplying with the local resistivity ρ, the impedance contribution or impedance volume density of each voxel can be found. The impedance contribution from a sub-volume is found from [Eq.3] if the integration is done over that specific volume. If the current density and the impedance volume density are known for each voxel, the potential drop caused by a voxel (or all voxels in a volume) can be found. It follows from this that the ratio of the potential drop between two equipotential lines to the total potential also gives the ratio of impedance contribution of this sub-volume to the total impedance. In a two-electrode setup, a potential plot is an easy way to display the sensitivity field.

The system impedance is expressed as [Eq.5] where $\boldsymbol{I}_{reci}$and ρ are constants. $\boldsymbol{I}_{reci}$ and ρ are used as "common" or generic entities representing saline and double layer to simplify this expression), the sensitivity field outer limit could be expressed by just plotting the electric potential distribution. The sensitivity field outer limit will be given within 97% of the accessible range of the results.

3. Results

In Figures 9 and 10 the impedance **Z** (Z' and Z'') is plotted as a function of the distance between needle tip and the neutral plate. Figures 9 and 10 have been compared as a quick test for FE-model validity. Z' is the real part and Z'' the imaginary part of **Z.**

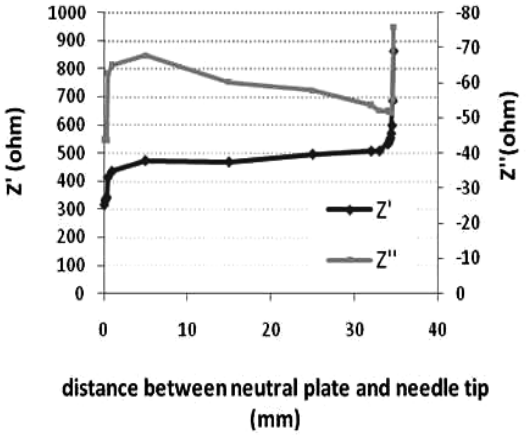

Figure 9. Results from FE-model plotting Z' and Z'' as a function of distance between neutral plate and needle tip. These results are in agreement with the results presented in figure 10.

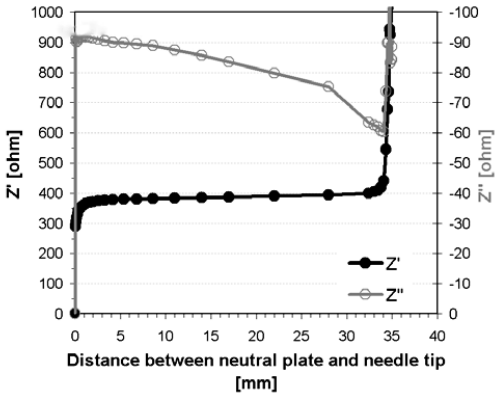

Figure 10. Shows the results from the lab-measurements (Kalvøy *et al.* 2009). Both vertical axes are shown with units ohm. The horizontal axis shows the distance between the needle tip and the neutral plate in millimetres

To calculate and display the sensitivity field the following approach was chosen: find the saline solution volume (with EPI included) corresponding to 97 % of the measured impedance. Then make a graphical illustration of the potentials between 100 % and 3 % (from 1.0 to 0.03 volts). This is shown in the following figure:

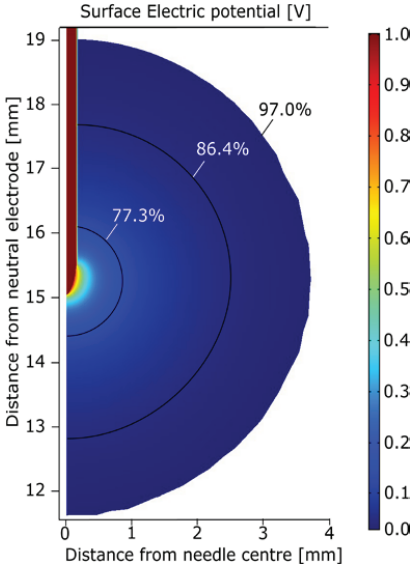

Figure 11. "97 %-zone" i.e. Electrical potential distribution and sensitivity field. Needle tip is at this point 15 mm from neutral plate. This figure shows that the sensitivity field is a sphere with an approximate radius of 3.75 mm. The vertical left scale has unit millimetres. The scale to the right shows a voltage factor, i.e. the value 1.0 is the maximum voltage and found at the needle electrode.

All needle positions, measured as distance from neutral plate, in the range from 4 to 30 mm showed a sensitivity field as in Figure 11. For distances outside this range the spherical shape was lost in accordance with the findings as shown Figure 9 and 10; the needle detects the object that has protruded its sensitivity zone.

4. Discussion

Figure 9 and 10 shows that the electrical properties of the lab-model are well described by the FE-model.

Figure 11 gave a 97 % sensitivity radius of 3.75 mm in saline. The inner equipotential line showed that the volume within one mm radius corresponds to 77.3 % of the measured impedance. In other words, we could have replaced the neutral electrode in the bottom of the tank with a spherical electrode of radius 3.75 mm, centered in the middle of the needle tip. The total measured impedance in the set-up would only be reduced by 3 %. In Kalvøy et al. 2009 we had to move the needle one third into this sensitivity zone, approximately 2.6 mm from the neutral plate, to obtain a 97% reduction of the impedance. This was what we could expect since the neutral plate only intercepted the sensitivity zone from one side. The correlation between simulations and measurements was also confirmed in a comparison of figure 9 and 10; in both figures we found similar change in resistance (Z') and reactance (Z'') as the needle tip approached the boundaries at 0 mm and 35 mm.

The simplifications of the needle geometry described in Ch II sect B, are done to reduce the use of computer resources. In our opinion these simplifications were beneficial, as the results above were obtained with reasonable computation time on a regular computer and still in accordance with the required FE-model quality as described in [Eq.4]

Still, some deviances can be found. Lab-model results show more even curves for needle distances between 5 to 30 millimeters than the FE-model due to the number of simulations. Each displayed value in Figure 9 is based on a separate FE-model. To reduce the total number of simulations only a few models have been made for the needle distances between 5 and 30 millimeters.

Deviances between the measured impedance (Z) in the lab-model and calculated impedance in the FE-model can probably be reduced by further fine-tuning of the material constants in the EPI. Such refinements are continuously in focus as we carry on our work on this modeling.

It is desirable to be able to do early-stage-FE-modeling without the close connections to a lab model, but as shown through this work, the FE-modeling process needs supportive lab-measurements.

5. Conclusion

It has been shown that the sensitivity field in a measuring system involving a needle electrode can be modelled, solved and described by a Finite Element model. In this system the sensitivity field has been estimated to be a spherically shaped zone with a radius of approximately 3.75 mm from needle metal surface. This result corresponds well with the observations from the needle-lab-model.

References

Kalvøy H, Frich L, Grimnes S, Martinsen Ø G, Hol P K and Stubhaug A 2009 Impedance based tissue discrimination for needle guidance *Physiol. Meas.* 30 129-40

Grimnes S, Martinsen Ø G 2008 Bioimpedance & Bioelectricity Basics *Academic Press San Diego* 188-91

Geselowitz D B 1971 An application of electrocardiographic lead theory to impedance plethysmography *IEEE Trans Biomed Eng* 18 38-41

Cooper R 1946 The electrical properties of salt-water solutions over the frequency range 1-400 Mc/s *J inst Elect Eng* 93 69-75

Mcadams E T, Lackermeier A, Mclaughlin J A, Macken D and Jossinet J 1995 The Linear and Nonlinear Electrical-Properties of the Electrode-Electrolyte Interface *Biosensors & Bioelectronics* 10 67-74

COMSOL Multiphysics Manual 2008 AC/DC Review of Electromagnetics *COMSOL Ver 3.5* 123-48

Cao H, Tungjitkusolmun S, Choy Y B, Tsai J Z, Vorperian V R and Webster J G 2002 Using electrical impedance to predict catheter-endocardial contact during RF cardiac ablation *IEEE Trans. Biomed. Eng*. 49 247–53

Kinouchi Y, Iritani T, Morimoto T and Ohyama S 1997 Fast in vivo measurements of local tissue impedances using needle electrodes *Med. Biol.Eng.Comput*. 486–92

Tsui BC, Wagner A, Finucane B 2004 Electrophysiologic effect of injectates on peripheral nerve stimulation. *Reg. Anesth. Pain Med* 29 189 –93

Sauter A.R., Dodgson M.S., Kalvøy H., Grimnes S., Stubhaug A, Klaastad Ø 2009 Current threshold for nerve stimulation depends on electrical impedance of the tissue: A study of ultrasound-guided electrical nerve stimulation of the median nerve. *Anesth. Analg* 108 (4) 1338-43

King J C, Dumitru D, Nandedkar S 1998 Concentric and single fibre electrode spatial recording characteristics, *Muscle & Nerve* 20 (12) 1525 – 33

VI

Invasive electrical impedance tomography for blood vessel detection

Ø.G. Martinsen[1,2], H. Kalvøy[1,2], S. Grimnes[1,2], B. Nordbotten[1], P.K Hol[3], E. Fosse[3], H. Myklebust[4], L.B. Becker[5]

[1]*Department of Physics, University of Oslo, Norway*

[2]*Department of Biomedical and Clinical Engineering, Oslo University Hospital, Norway*

[3]*The Interventional Center, Oslo University Hospital, Norway*

[4]*Laerdal Medical AS, Stavanger, Norway*

[5]*Department of Emergency Medicine, Hospital of the University of Pennsylvania, Philadelphia, USA*

Abstract: We present a novel method for localization of large blood vessels using a bioimpedance based needle positioning system on an array of ten monopolar needle electrodes. The purpose of the study is to develop a portable, low cost tool for rapid vascular access for cooling and controlled reperfusion of cardiac arrest patients. Preliminary results show that localization of blood vessels is feasible with this method, but larger studies are necessary to improve the technology.

Keywords: Electrical bioimpedance, needle electrode, invasive impedance tomography, cardiac arrest, cooling, reperfusion.

INTRODUCTION

Despite investments in research, training, equipment and infrastructure, survival from unexpected cardiac arrest has been virtually unchanged over the past couple of decades. On average, the survival rate is approximately 5 % in the USA/Europe, but can even be as low as 2 % in the bigger cities or above 20 % in those cities with the best implementation of science and education [1,2].

Time from cardiac arrest until cardiopulmonary resuscitation and defibrillation is one factor influencing survival. Another factor affecting survival is reperfusion injury. Cell death does not only take place as a result of ischemia, but even more as a function of reperfusion. Given the situation of sudden cardiac arrest, there is now evidence to suggest that most of the cell death and subsequent irreversible organ damage takes place as a consequence of uncontrolled reperfusion [3]. With controlled reperfusion, where there is full control of flow, pressure and composition of the reperfusing fluid, cell and organ damage can be substantially reduced.

A third factor that can improve survival is induced hypothermia. We know that therapeutic hypothermia is beneficial after cardiac arrest, and that intra-arrest cooling is beneficial both with respect to defibrillation success and survival to discharge from hospital. Cooling also seems to slow down the speed of cell death caused by reperfusion after cardiac arrest [4].

Hence, both rapid intra-arrest cooling and controlled reperfusion are interventions which may substantially extend the time window of opportunity after cardiac arrest, drowning or trauma. A prerequisite for achieving this, however, is the development of new methods for obtaining vascular access in a secure and effective manner.

In this paper we present a novel method for localization of large blood vessels using a bioimpedance based needle positioning system reported earlier [5]. An array of ten needles is plunged into the tissue and then stepped out again while electrical impedance spectra are recorded at each step for all ten needles. Different tissue types, such as blood, muscle or fat, will have characteristic impedance spectra and we can hence continuously determine what sort of tissue the needle tips are in. The basic idea is then to use needles located in large blood vessels as guides for cannulae to obtain vascular access.

Materials and methods

We have earlier reported on a new method for impedance-based tissue discrimination for needle guidance [5]. This method is based on sending a small sensing current through the needle for measurement of electrical impedance in a three-electrode setup. Due to the small cross section and hence high current density on the tip of the needle, the measured impedance will be totally dominated by the volume within a radius of approximately 2 mm from the needle tip.

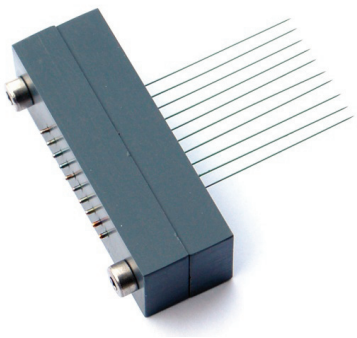

Fig. (1) Array of ten Viasys Healthcare Teca needles.

In this study we constructed an array of 10 Teca Monopolar Needle Electrodes (37mm x 28G) from Viasys Healthcare, mounted in a plastic block (figure 1). The shaft of the needles is electrically insulated, leaving only the sharp tip in galvanic contact with the tissue. The center-to-center distcance between the needles was 3 mm.

The study was approved by the Institutional Animal Care and Use Committee. The animals were supplied by the Centre for Comparative Medicine, Rikshospitalet University Hospital, Oslo, Norway. The femoral artery and vein of an anesthetized pig were located by ultrasound. The array was then pushed into the same region across the artery and vein until the plastic block was in contact with the pig skin (approx. 37 mm depth). The needles were connected through a Keithley 7001/7011S multiplexer to a Solartron 1260+1294 impedance analyzer. Each needle then served as a measuring electrode in a three-electrode system, where the reference and counter current electrodes were Ambu “Blue Sensor Q” ECG electrodes on the pig skin. After the insertion of the needles, the electrical impedance of each needle tip was measured successively with the Solartron system, using an applied voltage of 30 mV rms and frequencies between 10 Hz and 1 MHz. Then a 3 mm Plexiglas spacer was inserted between the plastic block and the pig skin, so that the needles were pulled out 3 mm. A new frequency scan was then performed on all needles, a new spacer introduced, then another frequency scan, etc. In this way a ten by ten matrix of impedance curves was attained.

Figure 2 shows an example of single needle measurements in different tissue types as described by Kalvøy *et al.* [5]. Frequencies up to at least 10 kHz are dominated by electrode polarization impedance and do not represent intrinsic biomaterial electrical properties. However, it is obvious that also the electrode impedance is tissue dependent, as pointed out by Kalvøy *et al.* [5] so the low frequency part of the spectra are also of interest for tissue discrimination.

As a first attempt of an invasive impedance tomography plot, we simply plotted the phase angle at 316 kHz for each pixel in the matrix. The chosen frequency is also in accordance with the findings of Salazar *et al.* [6]. The plotting was done in Mathematica 7 (Wolfram Research) using a “ListDensityPlot” with third order polynomial interpolation and a red-to-blue color map. Figure 3 shows the result together with a section of the ultrasound image from approximately the same area.

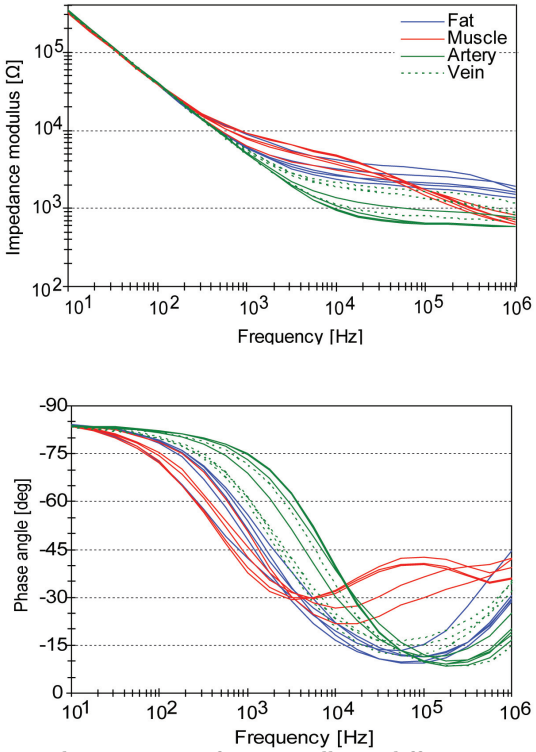

Fig. (2) Impedance spectra of Teca needles in different tissue types.

Discussion

The phase angle plot in figure 3 shows resemblance to the ultrasound image. The artery comes out quite clear, but with a somewhat oblate shape. The vein has a lower phase angle leading to a lighter red color.

As shown in figure 2, venous blood is more similar to fat in this frequency range so the light red areas in the lower and left part of the plot are more difficult to interpret. It could be bleeding (the acquisition of the data for the image took more than an hour) or fatty tissue.

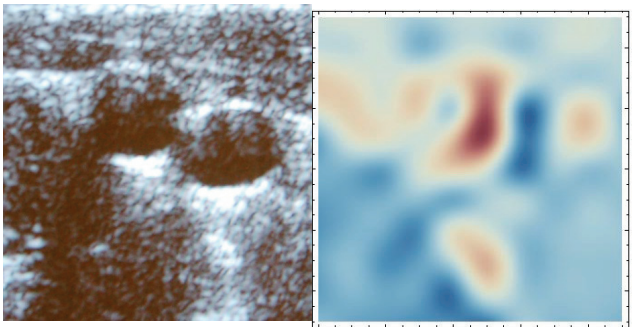

Fig. (3) Ultrasound image and plot of impedance phase angle at 316 kHz from approximately the same femoral area of an anesthetized pig, showing an artery (left) and a vein.

Conclusion

These preliminary result show that needle array measurements may prove valuable as a tool to guide needles into particular tissue types, such as blood vessels. Producing an image is not a necessary step in such an application, but it represents a convenient way of assessing the method. To our knowledge, this is the first time a percutaneous, invasive, electrical impedance tomography image is presented. The quality of the image, and hence the method, will probably be greatly improved when multivariate methods are used for classification of the tissue. Furthermore, when the proper multivariate model is developed, the instrumentation can probably be simplified to using only a few simultaneous measuring frequencies, thus significantly reducing the acquisition time.

References

[1] G. Nichol, E. Thomas, C.W. Callaway, *et al.*, "Regional variation in out-of-hospital cardiac arrest incidence and outcome", *JAMA*, vol. 300**,** pp. 1423-31, 2008.

[2] ILCOR, International Liaison Committee on Resuscitation, "International Consensus on Cardiopulmonary Resuscitation and Emergency Cardiovascular Care Science with Treatment Recommendations. Part 2: Adult basic life support", *Resuscitation*, vol. 67, pp. 187-201, 2005.

[3] T.L. Vanden Hoek, Y. Qin, K. Wojcik, C.Q. Li, Z.H. Shao, T. Anderson, L.B. Becker, and K.J. Hamann, "Reperfusion, not simulated ischemia, initiates intrinsic apoptosis injury in chick cardiomyocytes", *Am. J. Physiol. Heart Circ. Physiol.,* vol. 284, pp. H141-50, 2003.

[4] B.S. Abella, D. Zhao, J. Alvarado, K. Hamann, T.L. Vanden Hoek, and L.B. Becker, "Intra-arrest cooling improves outcomes in a murine cardiac arrest model", *Circulation,* vol. 109, pp. 2786-91, 2004.

[5] H. Kalvøy, L. Frich, S. Grimnes, Ø.G. Martinsen, P.K. Hol, and A. Stubhaug, "Impedance-based tissue discrimination for needle guidance", *Physiol. Meas.,* vol. 30, pp. 129-40, 2009.

[6] Y. Salazar, J. Cinca, and J. Rosell-Ferrer, "Effect of electrode locations and respiration in the characterization of myocardial tissue using a transcatheter impedance method", *Physiol. Meas.,* vol. 25, pp. 1095-1103, 2004.